detected multiple nodules in both lungs, and the mice showed reduced survival (Figure 3D, E). Histological examination of lung tumors in the transgenic mouse lines generally demonstrated adenocarcinomas with papillary/lepidic growth pattern (Figure 3C). These lesions were shown to be invasive adenocarcinomas with moderate mitotic activity as revealed by positive Ki-67 staining (Figure S6A). However, in some cases of TgB lines, we observed accumulation of cytoplasmic mucin in tumor cells (Figure S6B).

Despite the presence of multiple tumors in the lungs of the transgenic mice, we failed to detect distant metastasis at necropsy in TgA, B and C mice. Thus, it is likely that expression of *EZR-ROS1* alone is not sufficient to render the cancer cells metastatic.

Discussion

The present study identified *EZR-ROS1* as a pivotal driver oncogene in lung carcinogenesis. Ezrin is ubiquitously expressed in many tissues. In the *EZR-ROS1* fusion detected by RNA sequencing of LADC cases, 5′ portion of *EZR* causes aberrant overexpression of kinase domain of *ROS1*. No evident effect to the transcript levels of the 3′ portion of *EZR* was observed. This might be ascribable to the excess expression of the wild type *EZR* over the fusion gene. We also revealed that ROS1 kinase activation in this fusion requires the N-terminal FERM domain of EZR. FERM associates with many different proteins including phospholipids, the scaffolding proteins EBP50 and E3KARP, and other membrane-associated proteins that may regulate the dimerization or oligomerization of ezrin [21]. Many fusion kinase proteins, including ALK and RET, display constitutive tyrosine kinase activity attributable to dimerization domains in the amino-terminal fusion partner [6,22]. However, another ROS1 fusion protein, FIG-ROS1, which is found in human glioblastoma, cholangiocarcinoma and lung adenocarcinoma, showed no dimerization properties, instead existing as a monomer in the fusion protein despite retaining the coiled-coil domains and a leucine zipper [19]. Therefore, the molecular mechanisms underlying ROS1 activation by the FERM domain remains unclear.

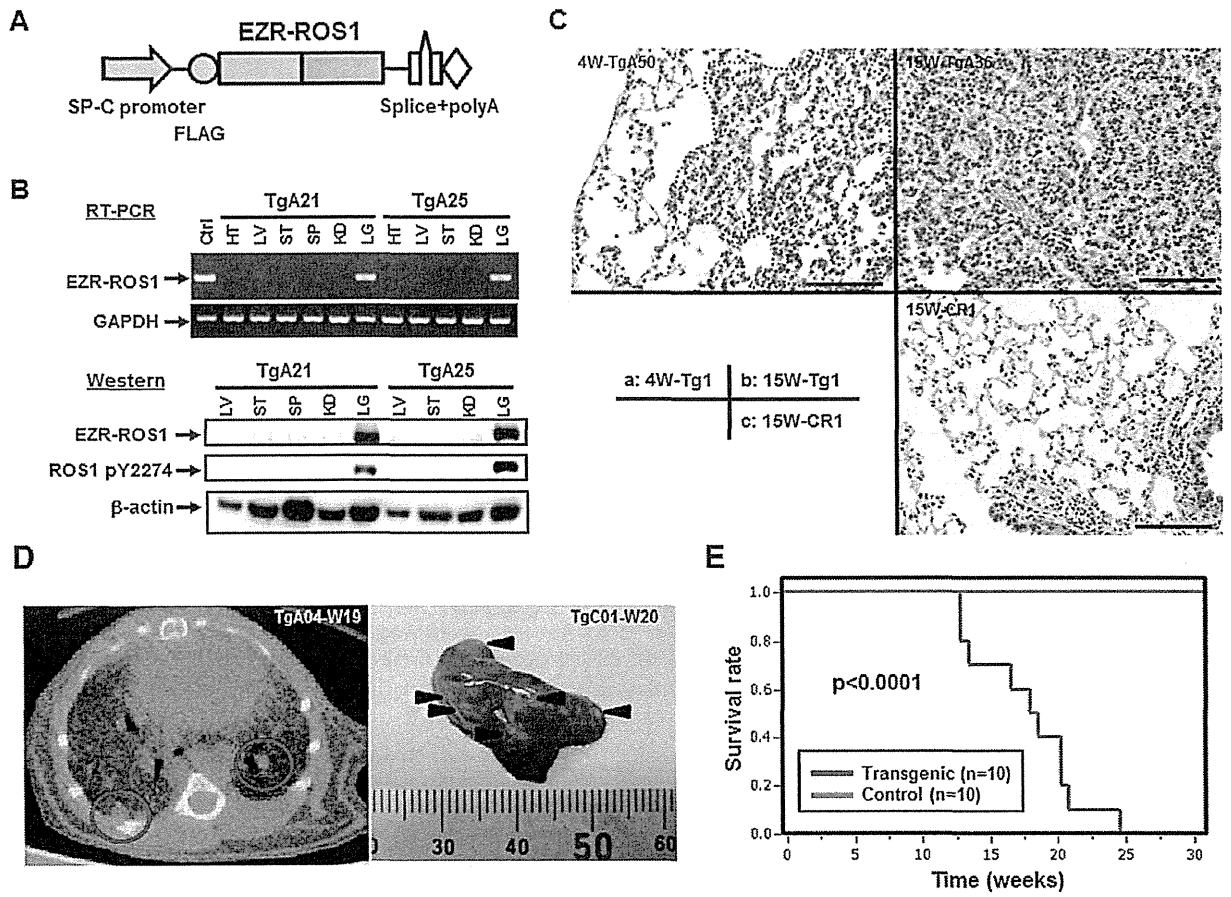

Figure 3. Alveolar epithelium-specific EZR-ROS1 expression generates lung adenocarcinoma *in vivo*. (A) Schematic presentation of the *SP-C/EZR-ROS1/polyA* transgene. (B) Expression of the exogenous *EZR-ROS1* gene in transgenic mice. RT-PCR (top) and immunoblot analysis (bottom) of mouse tissues revealed that EZR-ROS1 was specifically expressed in the lungs of two transgenic mice (TgA21 and TgA25). HT: heart, LV: liver, ST: stomach, SP: spleen, KD: kidney, LG: lung (C) Representative histological analysis of lung lesions in transgenic mice. Hematoxylin-eosin staining shows wide-spread lesions in both 4-week-old and 15-week-old fusion-positive mice. Tg: fusion-positive, CR: fusion-negative. Scale bar, 100 μm. (D) Computed tomography (left) of lungs in TgA04 mouse at week 19. Enhanced lesions in both lungs were detected. Multiple nodular lesions (right) were observed on the pleural surface of the lung in TgC01 mouse at necropsy. (E) Survival curves for transgenic and control mice generated using the Kaplan-Meier method.
doi:10.1371/journal.pone.0056010.g003

The transgenic mice showed an emergence of multiple adenocarcinoma nodules at an early point, and the fast progression of the tumors. These features are broadly similar to the *EML4-ALK* mouse model [8]. Several groups reported that mucinous cribriform pattern and signet ring cell are characteristic histological features of *EML4-ALK* positive human lung cancer [23–25]. Recently, we investigated histopathology of *ROS1*-fusion positive human lung cancers [16]. Although other researchers reported that signet ring cell feature was not common in *ROS1*-rearranged lung cancers [10], we found that 53% of the cases harbored mucinous cribriform or signet ring cell features similar to the *ALK*-rearranged lung cancers but that the rest showed papillary/lepidic growth pattern. *EZR-ROS1*-positive tumors seemed less well differentiated, and showed more frequently histological features of mucinous cribriform or signet ring cell. Our mouse model of *EZR-ROS1* lung cancer generally demonstrated papillary/lepidic growth pattern, but in some cases, we observed accumulation of cytoplasmic mucin in tumor cells, which quite resembles to the characteristic histology reported in *ROS1*-rearranged lung cancer. Currently we have no answer why only part of mice harbored tumors with mucin accumulation.

The *EZR-ROS1* fusion gene was specifically detected in lung cancer specimens of female never-smokers without *EGFR, KRAS,* and *ALK* alterations. It was estimated that ~2% of patients in White and Asian lung cancer cohorts had *ROS1*-rearrangements, which occur at significantly higher rates in younger, non-smoking, female individuals [10,11,16]. Although each alteration is infrequent, *ROS1* fusions with many kinds of 5′ partner genes (*CCDC6, CD74, EZR, FIG, KDELR2, LRIG3, SDC4, SLC34A2 and TPM3*) have been reported in lung, brain, biliary tract, and ovarian cancers [9–16,26–28]. These *ROS1*-rearranged tumors could be targeted therapeutically with specific kinase inhibitors, including crizotinib [10,14,27,29]. Two LADC patients had a remarkable clinical response to crizotinib [10,14]. Thus, our *EZR-ROS1* lung cancer animal model could be valuable for evaluating the therapeutic potential of these compounds and novel drugs as well as biological features of *ROS1*-rearranged lung cancer *in vivo*.

Materials and Methods

Clinical Samples

Tissue specimens from lung cancer patients were provided by the National Cancer Center Biobank, Japan. High-molecular weight genomic DNA and RNA were extracted from fresh frozen tumor specimens and non-cancerous lung tissues. Written informed consent was obtained from each patient. The study protocol was approved by the Ethical Committee of National Cancer Center, Tokyo, Japan.

Analysis of Whole-transcriptome Sequence Data

Insert cDNA libraries (150–200 bp) were prepared from 2 μg of total RNA using the mRNAseq Sample Preparation Kit (Illumina). The libraries were subjected to paired-end sequencing of 50 bp on the HiSeq2000 (Illumina), according to the manufacturer's instructions. Paired-end reads were mapped to known RNA sequences in the RefSeq, Ensembl, and LincRNA databases using the Bowtie program as described previously [30].

RT-PCR, Genomic PCR and Sequencing

Total RNA was reverse-transcribed to cDNA using Superscript III (Life Technologies). cDNA or genomic DNA was subjected to PCR amplification using Ex-Taq (Takara Bio) and primers EZR-e10-CF1 (GAAAAGGAGAGAAACCGTGGAG) and ROS1-e34-CR1 (TCAGTGGGATTGTAACAACCAG). The PCR products were directly sequenced by Sanger sequencing using the BigDye terminator kit (Life Technologies).

SNP Array CGH Analysis

Chromosomal copy number for the tumors was determined using high-resolution SNP arrays (GeneChip Mapping 250K-Nsp array, Affymetrix). Genomic DNA was labeled and hybridized to the SNP arrays according to the manufacturer's instructions, and copy numbers were calculated from the hybridization signals using the CNAG program [31].

Vector Cloning, and Generation of Deletion and Point Mutants

The coding region of *EZR-ROS1* cDNA was obtained by PCR amplification from LCY66 tumor cDNA using Phusion Taq polymerase (New England Biolabs) and primers EZR-H1F1 (CACCATGCCGAAACCAATCAATGTCCGAGTT) and ROS1-H1R1 (ATCAGACCCATCTCCATATCCACTGTG). *EML4-ALK* cDNA and *CCDC6-RET* cDNA were amplified from an *EML4-ALK*-positive primary lung cancer sample (E13;A20) and from a *CCDC6-RET*-positive primary lung cancer sample (C1;R12), respectively. The PCR products were subcloned into a pcDNA3.1D-V5-His plasmid (Life Technologies). Replacement of lysine with methionine at codon 491 in the *EZR-ROS1* gene was performed using a PrimeSTAR site-directed mutagenesis kit (Takara Bio). N-terminal deletion mutants of the FERM domain of *EZR-ROS1* cDNA were constructed by PCR using the primers EZR-FERM-AF (CACCATGGTGGCTGAGGAGCTCATC-CAGGACATC) and ROS1-H1R1 for DL1, EZR-FERM-BF (CACCATGATCAACTATTTCGAGATAAAAAACAAG) and ROS1-H1R1 for DL2, and EZR-FERM-CF (CACCATGAC-CATCGAGGTGCAGCAGATGAAGGC) and ROS1-H1R1 for DL3. The plasmids were transfected into NIH3T3 cells using Lipofectamine 2000 reagent (Life Technologies), and stable clones were isolated by G418 selection (0.7 mg/ml). For the colony formation assay, cells were embedded and cultured in 0.4% soft agar in triplicate and the number of colonies was counted after 21 days. Quantification of anchorage–independent growth under the condition with or without crizotinib (S1068, Selleck) and vandetanib (S1046, Selleck) after 9 days was performed with CytoSelect-96 kit (Cell Biolabs). The compound solution was added to the top layer of soft agar every 3 days.

Immunoblot Analysis

Whole cell lysates were extracted with CelLytic M reagent (#C2978, Sigma), and subjected to SDS-PAGE followed by blotting onto a PVDF membrane. Detection of Western blots was performed with the WesternBreeze Chemiluminescent Immunodetection kit (Life Technologies) using primary antibodies against ROS1 (#9202, Cell Signaling Technology), phosphorylated-ROS1 (Tyr2274) (#3078, Cell Signaling Technology), STAT3 (#610189, BD), phosphorylated-STAT3 (Tyr705) (#9138, Cell Signaling Technology), p44/42 MAPK (#4695, Cell Signaling Technology), phosphorylated-p44/42 MAPK (Thr202/Tyr204) (#9106, Cell Signaling Technology), Ezrin (#4135, Cell Signaling Technology), p53 (#6243, Santa Cruz), and b-actin (#A5441, Sigma).

Suppression of ROS 1 Kinase Activity of EZR-ROS1 by Crizotinib

Transfected NIH3T3 cells (empty vector, wild-type EZR-ROS1, KD/DL mutants) were serum starved for 2 hr, then

added for 2 h with 1% DMSO or 1 μM crizotinib, then the culture medium were changed with standard 10% FBS medium for 10 min. Whole cell lysates were subjected to immunoblot analysis.

Subcutaneous Transplantation in Immune-compromised Mice

A total of 1×10^6 cells were injected subcutaneously into nude mice (BALB/c-nu/nu, CLEA Japan). Mice were monitored daily for tumor formation. All animal procedures were performed with the approval of the animal ethical committee of the National Cancer Center.

Generation and Examination of *EZR-ROS1* Transgenic Mice

FLAG-tagged *EZR-ROS1* cDNA was subcloned into an *SPC-iNOS* plasmid (provided by Dr. Hagiwara), which included an *SPC* promoter and a polyadenylation signal, by replacing the *iNOS* fragment with the cDNA. The expression cassette with the *SPC* promoter was excised from the construct and injected into pronuclear-stage embryos of C57BL/6J mice (Unitech Japan). The copy number of the transgene was determined by Southern blot analysis of DNA from the tails of animals. Transgenic lines were maintained by backcrossing to C57BL/6 mice. Total RNA was isolated from the organs of transgenic mice and subjected to RT-PCR analysis to detect *EZR-ROS1*, endogenous *Ros1*, endogenous *Ezrin* and *Gapdh* mRNAs. To detect EZR-ROS1 protein, endogenous ROS1 and Ezrin in tissues, lysed homogenates were subjected to immunoblot analysis using anti-ROS1, anti-Ezrin and anti-β-actin antibodies. Examination of lung tumors in live animals was performed with an X-ray CT apparatus (eXplore micro-CT, GE Healthcare). Lung tissues were fixed in 10% formalin and paraffin-embedded. Hematoxylin-Eosin staining and immunohistochemistry for Ki67 was performed as previously described [32].

Supporting Information

Figure S1 Detection of *EZR-ROS1* genomic breakpoint junction. Electropherogram for Sanger sequencing of genomic fragments encompassing the *EZR-ROS1* breakpoint junction of LCY66 tumor. Genomic PCR products amplified by the EZR-e10-CF1 and ROS1-e34-CR1 primers were directly sequenced using the EZR-e10-CF1 primer. Numbers above the electropherogram indicate genomic position in chromosome 6 (human genome build 37.3). A genomic fragment of 35 bp of *EZR* intron 10 was inverted within the intron before the fusion to *ROS1* intron 33.
(PDF)

Figure S2 Detection of fusion gene transcripts in clinical samples by RT-PCR. Representative RT-PCR results showing fusion-positive and fusion-negative cases using primers EZR-e10-CF1 and ROS1-e34-CR1. M:molecular marker, NC: negative control. RT-PCR for wild-type *EZR* transcript (primers EZR-e4-CF1 and EZR-e7-CR1) and for *GAPDH* (primers for GAPDH-F and GAPDH-R) is also shown.
(PDF)

Figure S3 Copy number analysis of the transgene in transgenic mice. Genomic DNA was isolated from the tails of transgenic mice generated from pronuclear-stage C57BL/6J embryos. This gDNA was then subjected to Southern blot analysis with a PCR-amplified SPC promoter fragment of 464 bp, generated using primers SPC-pro-F and SPC-pro-R, as a probe. Control samples on the right were comprised of mouse genomic DNA with the indicated copies of the transgene per diploid genome. The ID numbers of mice positive for the transgene are shown at the top.
(PDF)

Figure S4 Gene expressions in transgenic mice. Expression of the genes indicated at left side was investigated by RT-PCR or immunoblot analysis. In RT-PCR, PCR cycles to amplify target genes were indicated at right side. Ezrin showed ubiquitous endogenous expression, however endogenous Ros1 expression was low. No expression of EZR-ROS1 fusion protein was detected in TgD line mice (*). SW480 was used as a negative control for fusion expression. HT: heart, LV: liver, ST: stomach, SP: spleen, KD: kidney, LG: lung.
(PDF)

Figure S5 Lung tumor development in transgenic mice. Lung tissues of TgA mice were cross-sectioned and histologically characterized. The number and size of lesions were surveyed in fusion-positive mice (Tg) and fusion-negative mice (CR) at 4 weeks and 15 weeks after birth. (a) Tumor lesions were classified along its size in diameter (mm), and counted. (b) Tumor occupancy was calculated from the deduced tumor area.
(PDF)

Figure S6 Histological characterization of lung tumors in transgenic mice. (A) Hematoxylin-eosin staining of a mouse lung showing invasive lung adenocarcinoma surrounding a pulmonary vessel (a1). Higher magnification of the tumor (a2). Positive Ki-67 staining in the tumor (a3). Scale bar, 100 μm. (B) Hematoxylin-eosin staining of a mouse lung showing cytoplasmic mucin in lung adenocarcinoma cells (b1). Higher magnification of the tumor (b2). Scale bar, 200 μm.
(PDF)

Acknowledgments

We thank Dr. K. Hagiwara (Saitama Medical University) for providing the SPC-iNOS plasmid, Drs. Y. Nanya and S. Ogawa (University of Tokyo) for providing the CNAG program, and Ms. N. Okada, H. Shimizu, A. Kokubu, T. Urushidate, S. Ohashi and W. Mukai for their excellent technical assistance.

Author Contributions

Conceived and designed the experiments: YA YT TS. Performed the experiments: YA H. Takahashi MM FH. Analyzed the data: YT YA TK HN NH. Contributed reagents/materials/analysis tools: KT AY HA H. Tsuda. Wrote the paper: YA YT TS.

References

1. Jemal A, Bray F, Center MM, Ferlay J, Ward E, et al. (2011) Global Cancer Statistics. CA Cancer J Clin 61: 69–90.
2. Janku F, Stewart DJ, Kurzrock R (2010) Targeted therapy in non-small-cell lung cancer - is it becoming a reality? Nat Rev Clin Oncol 7: 401–414.
3. Gerber DE, Minna JD (2010) ALK inhibition for non-small cell lung cancer: from discovery to therapy in record time. Cancer Cell 18: 548–551.
4. Lovly CM, Carbone DP (2011) Lung cancer in 2010: One size does not fit all. Nat Rev Clin Oncol 8: 68–70.
5. Sasaki T, Jänne PA (2011) New strategies for treatment of ALK-rearranged non–small cell lung cancers. Clin Cancer Res 17: 7213–7218.
6. Soda M, Choi YL, Enomoto M, Takada S, Yamashita Y, et al. (2007) Identification of the transforming EML4-ALK fusion gene in non-small lung cancer. Nature 448: 561–566.

7. Li D, Shimamura T, Ji H, Chen L, Haringsma HJ, et al. (2007) Bronchial and peripheral murine lung carcinomas induced by T790M-L858R mutant EGFR respond to HKI-272 and rapamycin combination therapy. Cancer Cell 12: 81–93.
8. Soda M, Takada S, Takeuchi K, Choi YL, Enomoto M, et al. (2008) A mouse model for EML4-ALK-positive lung cancer. Proc Natl Acad Sci U S A 105: 19893–19897.
9. Rikova K, Guo A, Zeng Q, Possemato A, Yu J, et al. (2007) Global survey of phosphotyrosine signaling identifies oncogenic kinases in lung cancer. Cell 131: 1190–1203.
10. Bergethon K, Shaw AT, Ou SH, Katayama R, Lovly CM, et al. (2012) ROS1 Rearrangements define a unique molecular class of lung cancers. J Clin Oncol 30: 863–870.
11. Takeuchi K, Soda M, Togashi Y, Suzuki R, Sakata S, et al. (2012) RET, ROS1 and ALK fusions in lung cancer. Nat Med. 18: 378–381.
12. Rimkunas VM, Crosby KE, Li D, Hu Y, Kelly ME, et al. (2012) Analysis of Receptor Tyrosine Kinase ROS1-Positive Tumors in Non-Small Cell Lung Cancer: Identification of a FIG-ROS1 Fusion. Clin Cancer Res 18: 4449–4457.
13. Seo JS, Ju YS, Lee WC, Shin JY, Lee JK, et al. (2012) The transcriptional landscape and mutational profile of lung adenocarcinoma. Genome Res 22: 2109–2119.
14. Davies KD, Le AT, Theodoro MF, Skokan MC, Aisner DL, et al. (2012) Identifying and Targeting ROS1 Gene Fusions in Non-Small Cell Lung Cancer. Clin Cancer Res 18: 4570–4579.
15. Govindan R, Ding L, Griffith M, Subramanian J, Dees ND, et al. (2012) Genomic landscape of non-small cell lung cancer in smokers and never-smokers. Cell 150: 1121–1134.
16. Yoshida A, Kohno T, Tsuta K, Wakai S, Arai Y, et al. (in press) ROS1-rearranged lung cancer: a clinicopathological and molecular study of 15 surgical cases. Am J Surg Path in press.
17. Maher CA, Kumar-Sinha C, Cao X, Kalyana-Sundaram S, Han B, et al. (2009) Transcriptome sequencing to detect gene fusions in cancer. Nature 458: 97–101.
18. Chishti AH, Kim AC, Marfatia SM, Lutchman M, Hanspal M, et al. (1998) The FERM domain: a unique module involved in the linkage of cytoplasmic proteins to the membrane. Trends Biochem Sci 23: 281–282.
19. Charest A, Kheifets V, Park J, Lane K, McMahon K, et al. (2003) Oncogenic targeting of an activated tyrosine kinase to the Golgi apparatus in a glioblastoma. Proc Natl Acad Sci U S A. 100: 916–921.
20. Mishra A, Weaver TE, Beck DC, Rothenberg ME (2001) Interleukin-5-mediated allergic airway inflammation inhibits the human surfactant protein C promoter in transgenic mice. J Biol Chem 276: 8453–8459.
21. Fehon RG, McClatchey AI, Bretscher A (2010) Organizing the cell cortex: the role of ERM proteins. Nat Rev Mol Cell Biol 11: 276–287.
22. Medves S, Demoulin JB (2012) Tyrosine kinase gene fusions in cancer: translating mechanisms into targeted therapies. J Cell Mol Med 16: 237–248.
23. Inamura K, Takeuchi K, Togashi Y, Hatano S, Ninomiya H, et al. (2009) EML4-ALK lung cancers are characterized by rare other mutations, a TTF-1 cell lineage, an acinar histology, and young onset. Mod Pathol 22: 508–515.
24. Mino-Kenudson M, Chirieac LR, Law K, Hornick JL, Lindeman N, et al. (2010) A novel, highly sensitive antibody allows for the routine detection of ALK-rearranged lung adenocarcinomas by standard immunohistochemistry. Clin Cancer Res 16: 1561–1571.
25. Yoshida A, Tsuta K, Nakamura H, Kohno T, Takahashi F, et al. (2011) Comprehensive histologic analysis of ALK-rearranged lung carcinomas. Am J Surg Pathol 35: 1226–1234.
26. Charest A, Lane K, McMahon K, Park J, Preisinger E, et al. (2003) Fusion of FIG to the receptor tyrosine kinase ROS in a glioblastoma with an interstitial del(6)(q21q21). Genes Chromosomes Cancer 37: 58–71.
27. Gu TL, Deng X, Huang F, Tucker M, Crosby K, et al. (2011) Survey of tyrosine kinase signaling reveals ROS kinase fusions in human cholangiocarcinoma. PLoS One 6: e15640.
28. Birch AH, Arcand SL, Oros KK, Rahimi K, Watters AK, et al. (2011) Chromosome 3 anomalies investigated by genome wide SNP analysis of benign, low malignant potential and low grade ovarian serous tumours. PLoS One 6: e28250.
29. Park BS, El-Deeb IM, Yoo KH, Oh CH, Cho SJ, et al. (2009) Design, synthesis and biological evaluation of new potent and highly selective ROS1-tyrosine kinase inhibitor. Bioorg Med Chem Lett 19: 4720–4723.
30. Totoki Y, Tatsuno K, Yamamoto S, Arai Y, Hosoda F, et al. (2011) High-resolution characterization of a hepatocellular carcinoma genome. Nat Genet 43: 464–469.
31. Nannya Y, Sanada M, Nakazaki K, Hosoya N, Wang L, et al. (2005) A robust algorithm for copy number detection using high-density oligonucleotide single nucleotide polymorphism genotyping arrays. Cancer Res 65: 6071–6079.
32. Yoshikawa D, Ojima H, Kokubu A, Ochiya T, Kasai S, et al. (2009) Vandetanib (ZD6474), an inhibitor of VEGFR and EGFR signaling, as a novel molecular-targeted therapy against cholangiocarcinoma. Br J Cancer 100: 1257–1266.

Lung Cancer 81 (2013) 371–376

Contents lists available at SciVerse ScienceDirect

Lung Cancer

journal homepage: www.elsevier.com/locate/lungcan

The utility of the proposed IASLC/ATS/ERS lung adenocarcinoma subtypes for disease prognosis and correlation of driver gene alterations

Koji Tsuta[a,*,1], Mitsumasa Kawago[a,b,1], Eisuke Inoue[c], Akihiko Yoshida[a], Fumiaki Takahashi[c], Hiroyuki Sakurai[b], Shun-ichi Watanabe[b], Masahiro Takeuchi[c], Koh Furuta[a], Hisao Asamura[b], Hitoshi Tsuda[a]

[a] Division of Pathology and Clinical Laboratory Division, National Cancer Center Hospital, Tokyo, Japan
[b] Division of Thoracic Surgery, National Cancer Center Hospital, Tokyo, Japan
[c] Department of Clinical Medicine (Biostatistics), School of Pharmacy, Kitasato University, Tokyo, Japan

ARTICLE INFO

Article history:
Received 19 March 2013
Received in revised form 12 June 2013
Accepted 24 June 2013

Keywords:
IASLC classification
Adenocarcinoma of the lung
ALK
EGFR
KRAS

ABSTRACT

Background: The present study aimed to determine the ability of the revised International Association for the Study of Lung Cancer (IASLC)/American Thoracic Society (ATS)/European Respiratory Society (ERS) classification of lung adenocarcinoma to predict patient survivals and driver gene alterations.
Patients and Methods: A reclassification of 904 surgically resected adenocarcinomas was performed. The results were statistically analyzed to examine the correlation between the classification and overall survival (OS) using Cox regression analyses, and integrated discrimination improvement (IDI) analyses.
Results: The 5-year OS rates for adenocarcinomas in situ (AIS) or minimally invasive adenocarcinoma (MIA) were 98%. Five-year OS rates of Lepidic-, acinar-, papillary-, micropapillary-, and solid-predominant adenocarcinomas was 93%, 67%, 74%, 62%, and 58%, respectively. The IDI estimates revealed that classification of ADC into the 7 subgroups had a higher estimated (0.0175) than did the combined histological grouping (AIS + MIA, lepidic + acinar + papillary, micropapillary + solid + others) (0.0111). Epidermal growth factor receptor mutations, *KRAS* gene mutations, and anaplastic lymphoma kinase gene alterations were statistically prevalent in papillary-predominant ($P = 0.00001$), invasive mucinous ($P = 0.00001$), and micropapillary- and acinar-predominant ($P = 0.00001$) adenocarcinomas, respectively.
Conclusions: The new classification reflects disease prognosis, and was also associated with driver gene alterations.

1. Introduction

Primary lung adenocarcinomas (ADC) have 4 architectural growth patterns: bronchioloalveolar, acinar, papillary, and solid [1,2]. Although approximately 80% of invasive ADCs include 2 or more of these patterns, most cases have been referred to as "mixed adenocarcinoma," based on the latest World Health Organization (WHO) 2004 classification [1,3]. Several current clinicopathological and molecular analyses have revealed that architectural growth patterns of lung ADCs are correlated with both patient survival and the gene mutation profiles of the tumors [3–5]. To improve the clinical utility of histological classification system, the International Association for the Study of Lung Cancer (IASLC), American Thoracic Society (ATS), and European Respiratory Society (ERS) have cooperatively organized an updated classification of lung ADCs [2].

In the IASLC/ATS/ERS classification [2], there are several major changes pertaining to surgically resected tumors: (1) the term bronchioloalveolar carcinoma (BAC) is no longer used and is, instead, referred to as a lepidic pattern; (2) ADC in situ (AIS) describes small (≤3 cm), solitary ADCs with pure lepidic growth, which have not invaded surrounding normal tissue; (3) minimally invasive ADC (MIA) describes small (≤3 cm) predominantly lepidic tumors with ≤0.5 cm of invasion; (4) invasive ADCs are now classified according to their predominant subtype; (5) micropapillary ADC was added as a subtype because of its poor prognosis; (6) the former mucinous BACs are now classified as invasive mucinous ADCs (IMA); and (7) the terms clear-cell and signet-ring ADC were changed from histological subtypes to cytological features. The ADC variants listed in the IASLC/ATS/ERS classification include invasive mucinous, colloid, enteric, and fetal adenocarcinomas.

* Corresponding author at: The Division of Pathology and Clinical Laboratory, National Cancer Center Hospital, 1-1 Tsukiji 5-chome, Chuo-ku, Tokyo 104-0045, Japan. Tel.: +81 3 3542 2511; fax: +81 3 3545 3567.
E-mail address: ktsuta@ncc.go.jp (K. Tsuta).
[1] These authors contributed equally to this study.

0169-5002/$ – see front matter © 2013 Elsevier Ireland Ltd. All rights reserved.
http://dx.doi.org/10.1016/j.lungcan.2013.06.012

Recently, 4 research groups analyzed the association between the IASLC/ATS/ERS classification scheme and survival [6–9]. These studies concluded that the IASLC/ATS/ERS classification identified histological subtypes of lung ADCs that were of significant prognostic value. However, one of these reports analyzed only stage I cases, and the population of the other reports was analyzed the 5-year overall survival (OS) rate. In addition, neither report analyzed the association between the IASLC/ATS/ERS classification and the major driver-gene alterations.

In the present study, we analyzed the association between the IASLC/ATS/ERS classification with survival and the ability of this classification scheme to predict gene abnormalities, such as *EGFR*, *KRAS*, or anaplastic lymphoma kinase (*ALK*) gene alterations, using a large series of surgically resected lung ADCs. We also analyzed the relevant T-stage of newly proposed AIS and MIA and describe the possible histological factors affecting the survival in T1 tumors.

2. Materials and methods

2.1. Study population

This study was approved by the Institutional Review Board. Tumor specimens, surgically resected from patients diagnosed with primary lung ADC between January 1998 and December 2002, were retrospectively reviewed. Clinical information was collected regarding the patients' ages, genders, smoking histories, and duration of any tumor recurrences and survival.

2.2. Histological analyses

The pathologic records of the specimens and all available hematoxylin and eosin (HE)-stained tissue sections, in addition to any available sections with special stains or immunohistochemical analyses, were reviewed. Pathological information, including maximum tumor sizes (in cm) and pathologic disease stages (p-stage), was collected. Staging was based on the guidelines of the 7th edition of the TNM classification for lung cancer [10].

All available HE-stained sections, for each case, were examined by 2 researchers blinded to the clinical details of the patient. Histological classification was performed according to the IASLC/ATS/ERS classification of lung ADCs [2]. Lymphovascular invasion was evaluated by examining sections stained with HE and/or the Elastica van Gieson method.

2.3. Analyses of the EGFR and KRAS mutational status, and ALK rearrangement

The mutational status of *EGFR* and *KRAS*, and *ALK* rearrangements were examined. Two common *EGFR* mutations, deletions in exon 19 (DEL) and a point mutation at codon 858 in exon 21 (L858R), and *KRAS* mutations in exons 1 and 2 were detected using high-resolution melting analysis [11]. *ALK* translocations were analyzed by immunohistochemistry, reverse transcription-polymerase chain reaction (RT-PCR), and/or fluorescence in situ hybridization assays, according to previously published methods [12].

2.4. Statistical analyses

Means, medians, ranges, and proportions were used as descriptive statistics. The association between driver gene alterations and ADC subtypes was analyzed by a logistic model adjusted for age, gender, and smoking status. The 5- and 10-year survival rates for each subtype were calculated by the Kaplan–Meier estimator. Among patients with T1 tumors, survival was compared with the clinicopathologic factors using the Cox model.

To examine the significance of each ADC subtype, the Cox models, with and without subtypes, were constructed and likelihood ratio testing of the model was performed. These models were also adjusted by age, gender, stage, and lymphovascular invasions. To assess the improvement of the model performance by adding ADC subtype, the integrated discrimination improvement (IDI) [13] value was calculated and used to evaluate the 10-year risk of death. The IDI value is equivalent to the difference in R2 of the models, with and without subtypes. It is possible to evaluate the gain in predictive ability by adding subtypes to the model. The statistical significance of the IDI values was assessed by examining their 95% confidence intervals, which were calculated by the percentile bootstrap method [13].

All tests were two sided with a 0.05 type I error. *P*-Values were reported without multiple comparison adjustments. Data were analyzed with R version 2.14 [14].

3. Results

3.1. Patient characteristics

Tumor specimens from 956 patients with an original diagnosis of primary lung ADC were reviewed. Patients were excluded if they had received preoperative therapy ($n=13$), did not have specimens available for review ($n=9$), had pleural disseminations or malignant effusions ($n=15$), or were reclassified with lung tumors of histological types other than ADC ($n=15$). Therefore, the final cohort consisted of 904 patients with lung ADCs.

In this study population, there were 445 (49%) women and 459 (51%) men. The median age was 63 years (range: 23–89-years). All patients had provided documentation of their smoking history; 446 (49.3%) patients were never smokers and 458 (50.7%) were former or present smokers at the time of their diagnoses. Tumor sizes ranged from 0.4 to 17.5 cm (mean, 2.7 cm). Lymphovascular invasions were noted in 440 (48.7%) cases. Five hundred six patients had p-T1 disease, 297 had p-T2, 83 had p-T3 disease, and 18 had p-T4 disease. Lymph node status was recorded in 869 (96.1%) patients, and metastasis was observed in 217 (25%). Five hundred seventy-nine patients had p-stage I disease, 149 had p-stage II disease, and 141 had p-stage III disease.

Among the 904 cases, 69 (8%) cases were AIS and 33 (4%) cases were minimally invasive adenocarcinoma (MIA). Among the 757 cases of invasive adenocarcinoma, the most prevalent variant was papillary predominant ADC (338 cases; 37%; PPA), followed by lepidic-predominant ADC (136 cases; 15%; LPA), solid with mucin production-predominant ADC (124 cases; 14%; SPA), acinar-predominant ADC (98 cases; 11%; APA), and micropapillary-predominant ADC (61 cases; 7%; MPA). There were 45 (5%) cases of IMA, but no cases of mucinous AIS or MIA, or colloid, fetal, or enteric ADC. Clinical and pathological characteristics subdivided by IASLC/ATS/ERS histological subtype were shown in Table 1.

3.2. Survival analysis

Tumor recurrence was observed in 272 (30.1%) of the 904 patients. The mean follow-up time for all 904 patients was 8.2 years (range, 0.19–13.8 years), with 569 (62.9%) patients still alive at the time of the writing of this report. The 5-year OS was 76% for the 904 patients. None of 102 patients with AIS or MIA demonstrated recurrence.

The 5- and 10-year OS rates for AIS and MIA was 98% and 94%, respectively. These OS rates included 6 deaths by other cancers or diseases; therefore, the 5- and 10-year disease-specific survival rates were both 100%. The 5- and 10-year OS rates for the different subtypes, respectively, were 93% and 85% for LPA; 67% and 47% for

Table 1
Clinical and pathological characteristics to IASLC/ATS/ERS histological subtype.

	AIS or MIA	Lepidic	Acinar	Papillary	Micropapillary	Solid	IMA	Total
Number (%)	102(11.3)	136(15.1)	98(10.8)	338(37.4)	61(6.7)	124(13.7)	45(5.0)	904(100)
Gender								
Female (%)	56(55)	80(58.8)	46(46.9)	171(50.6)	30(49.2)	38(30.6)	24(53.3)	445(49.2)
Male (%)	46(45)	56(41.2)	52(53.1)	167(49.4)	31(50.8)	86(69.4)	21(46.7)	459(50.8)
Age (year)								
Median	63	65	62	64	62	64	68	63
Range	42–78	23–88	30–81	28–88	26–82	32–89	43–89	23–89
Smoking								
Never (%)	61(59.8)	84(61.8)	46(46.9)	171(50.6)	25(41)	33(26.6)	26(57.8)	446(49.3)
Former/Present (%)	41(40.2)	52(38.2)	52(53.1)	167(49.4)	36(59)	91(73.4)	19(42.2)	458(50.7)
Tumor size (cm)								
Median	1.2	1.9	2.8	2.5	2.5	2.5	3.7	2.7
Range	0.4–2.8	0.7–7.0	0.7–8.0	0.5–13	0.8–9.5	1.0–9.0	0.8–17.5	0.4–17.5
Lymphovascular invasion								
Negative	102(100)	122(89.1)	28(28.6)	135(40.1)	17(27.9)	18(14.5)	42(93.3)	464(51.3)
Positive	0	15(10.9)	70(71.4)	202(59.9)	44(72.1)	106(85.5)	3(6.7)	440(48.7)
Tumor stage								
T1	102(100)	112(82.4)	36(36.7)	167(49.4)	26(42.6)	41(33.1)	22(48.9)	506(56.0)
T2	0	24(17.6)	45(45.9)	133(39.3)	23(37.7)	63(50.8)	9(20.0)	297(32.9)
T3	0	0	16(16.3)	31(9.2)	7(11.5)	17(13.7)	12(26.7)	83(9.2)
T4	0	0	1(1.0)	7(2.1)	5(8.2)	3(2.4)	2(4.4)	18(2.0)
Lymph node status								
Negative	87(100)	126(96.9)	59(61.5)	235(71.2)	37(60.7)	67(55.4)	41(93.2)	652(75.0)
Positive	0	4(3.1)	37(38.5)	95(28.8)	24(39.3)	54(44.6)	3(6.8)	217(25.0)
Pathological stage								
I+II (%)	87(100)	130(100)	75(78.1)	264(80.0)	43(70.5)	89(73.6)	40(90.9)	728(83.8)
III+IV (%)	0	0	21(21.9)	66(20.0)	18(29.5)	32(26.4)	4(9.1)	141(16.2)

Abbreviations: IASLC, International Association for the Study of Lung Cancer; ATS, American Thoracic Society; ERS, European Respiratory Society; AIS, adenocarcinoma in situ; MIA, minimally invasive adenocarcinoma; IMA, invasive mucinous adenocarcinoma.

APA; 74% and 57% for PPA; 62% and 47% for MPA; 58% and 41% for SPA; and 76% and 63% for IMA (Fig. 1).

A univariate analysis indicated that gender ($P<0.001$), age ($P<0.001$), smoking history ($P=0.003$), tumor stage ($P<0.001$), and lymphovascular invasion ($P<0.001$) were significantly associated with OS (Table 2). To analyze the significance of ADC histological classifications, the previously reported histological groupings, (AIS + MIA, LPA + APA + PPA, MPA + SPA + other variants) and the 7 new subtypes were analyzed. The likelihood ratio test for the model with and without 7 subtypes was statistically significant ($P=0.004$), and that of the model with and without combined subtypes was also significant ($P=0.001$). The IDI estimates revealed that classification of ADC into the 7 subgroups had a higher estimated (0.0175, 95% confidence interval [0.0052, 0.0378]) than did the combined histological grouping (0.0111 [0.0004, 0.0226]).

To determine whether or not AIS + MIA tumors should be classified as T1 or Tis, the estimated OS functions were compared among AIS + MIA, conventional T1 tumors (including AIS + MIA), and those excluding AIS + MIA. The 5- and 10-year OS rates for AIS + MIA, conventional T1 tumors (including AIS + MIA), and those excluding AIS + MIA tumors were 98.0% and 93.6%, 86.7% and 77.7%, and 83.9% and 73.6%, respectively. There were statistical differences between

Table 2
Impacts of valuables on patient overall survival estimated by Cox's univariate analysis.

Variables	HR	95%CI	*P*
Gender			<0.001
Male vs Female	1.553	1.249–1.930	
Age	1.027	1.016–1.040	<0.001
Smoking			0.003
Former/Present vs Never	1.391	1.120–1.726	
Stage			<0.001
III vs I + II	5.640	4.485–7.095	
Lymphovascular invasion			<0.001
Positive vs Negative	4.377	3.420–5.603	

HR, hazard ratio; CI, confidence interval.

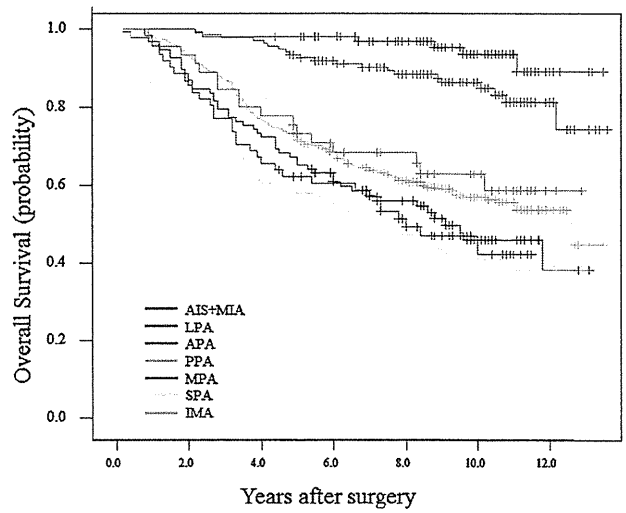

Fig. 1. Overall survival (OS) curves for each subtype. The 5- and 10-year OS rates for 102 adenocarcinoma in situ (AIS) or microinvasive (MIA) cancers were 98% and 94%, respectively (blue line). The 5- and 10-year OS rates for 136 lepidic predominant adenocarcinoma (LPA)s were 93% and 85%, respectively (green line). The 5- and 10-year OS rates for 98 acinar predominant adenocarcinoma (APA)s were 67% and 47%, respectively (purple line). The 5- and 10-year OS rates for 338 papillary predominant adenocarcinoma (PPA)s were 74% and 57%, respectively (gray line). The 5- and 10-year OS rates for 61 micropapillary predominant adenocarcinoma (MPA)s were 62% and 47%, respectively (red line). The 5- and 10-year OS rates for 124 solid predominant adenocarcinoma (SPA)s were 58% and 41%, respectively (yellow line). The 5- and 10-year OS rates for 45 invasive mucinous adenocarcinoma (IMA)s were 76% and 63%, respectively (aqua line). *Abbreviations*: Ref, reference; AIS, adenocarcinomas in situ; MIA, minimally invasive adenocarcinoma; PPA, papillary predominant adenocarcinoma; APA, acinar predominant adenocarcinoma; SPA, solid predominant adenocarcinoma; MPA, micropapillary predominant adenocarcinoma; HR, hazard ratio; CI, confidence interval. (For interpretation of the references to colour in this figure legend, the reader is referred to the web version of this article.)

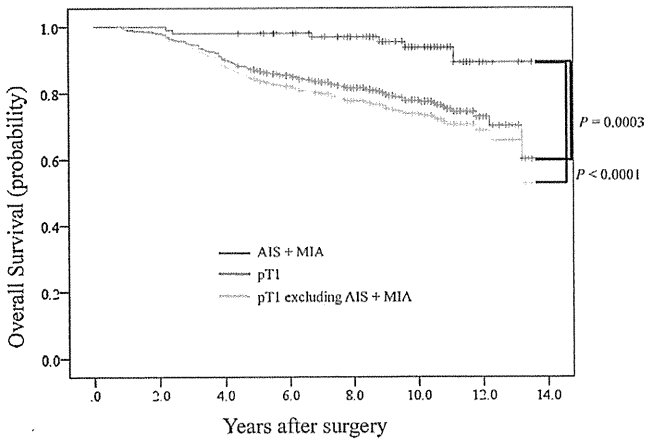

Fig. 2. Overall survival (OS) curves of patients with adenocarcinomas in situ (AIS) + minimally invasive adenocarcinoma (MIA). Statistically significant differences are observed between AIS + MIA (blue line) and pathological T1 tumors (green line, $P = 0.0003$) and between AIS + MIA and pathological T1 tumors, excluding AIS and MIA (gray line, $P < 0.0001$). (For interpretation of the references to colour in this figure legend, the reader is referred to the web version of this article.)

AIS + MIA tumors and T1 tumors excluding AIS + MIA ($P < 0.0001$) and between AIS + MIA tumors and conventional T1 tumors including AIS + MIA ($P = 0.0003$), based on patient survival (Fig. 2).

The significance of lymphovascular invasions on OS was analyzed in the 506 T1 cases. The 5- and 10-year OS rates for T1 tumors, T1 tumors without lymphovascular invasion, and T1 tumors with lymphovascular invasions were 86.7% and 77.7%, 94.0% and 87.5%, and 69.4% and 55.1%, respectively (Fig. 3). The OS rates of T1 tumors with lymphovascular invasions corresponded to those observed with the T2a tumors (5- and 10-year OS rates were 65.0% and 45.6%, respectively). There were significant statistical differences between T1 tumors and T1 tumors with lymphovascular invasion ($P < 0.0001$) and T1 tumors and T1 tumors without lymphovascular invasion ($P = 0.0003$). And there was no statistical significant differences between T1 tumors with lymphovascular invasion and T2a ($P = 0.065$).

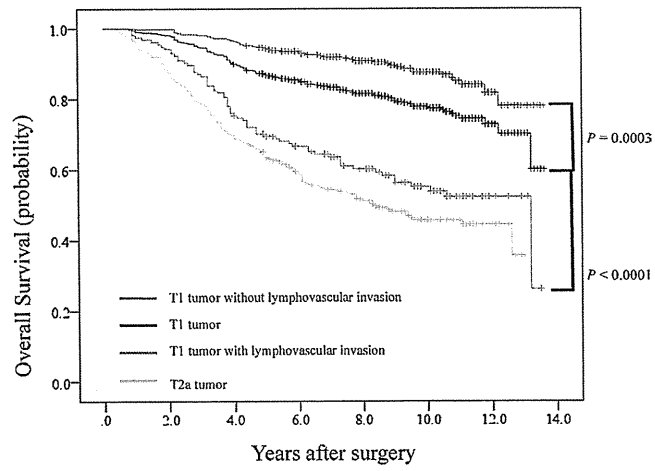

Fig. 3. Significance of lymphovascular invasion in pathological T1 tumors. Statistically significant differences are observed between T1 tumors without lymphovascular invasion (blue line) and T1 tumors (purple line, $P = 0.0003$) and between T1 tumors with lymphovascular invasion (purple line) and T1 tumors (green line, $P < 0.0001$). (For interpretation of the references to colour in this figure legend, the reader is referred to the web version of this article.)

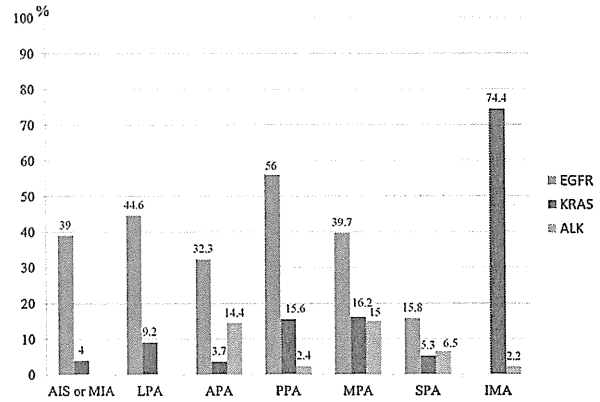

Fig. 4. Gene mutation detection rates for each histological subtype. Papillary-predominant adenocarcinomas (PAP) are independent predictors of epidermal growth factor receptor (*EGFR*) mutation (blue bar) positivity ($P = 0.00001$). Invasive mucinous adenocarcinomas (IMA) are independent predictors of *KRAS* mutation (red bar) positivity ($P = 0.00001$). Acinar-predominant adenocarcinomas (APAs) and micropapillary-predominant adenocarcinoma (MPAs) are independent predictors of anaplastic lymphoma kinase (*ALK*) rearrangement (green bar) positivity ($P = 0.0002$ and 0.00001, respectively). However, *ALK* translocations are not observed in adenocarcinoma in situ (AIS) + microinvasive adenocarcinoma (MIA) or lepidic predominant adenocarcinoma (LPA). (For interpretation of the references to colour in this figure legend, the reader is referred to the web version of this article.)

3.3. Mutational analysis

EGFR mutations were detected in 356 (40.5%) of the 880 analyzed cases, *KRAS* mutations were detected in 96 (11.1%) of the 862 analyzed cases, and *ALK*-translocations were detected in 40 (4.5%) of the 893 analyzed cases. These driver gene alterations were mutually exclusive. The distribution of these gene alterations, relative to each ADC subtype, is depicted in Fig. 4. The *EGFR* mutation was most prevalent in PPAs (56.0%), followed by LPAs (44.6%), MPAs (39.7%), AIS + MIAs (39.0%), APAs (32.3%), and SPAs (15.8%). There were no *EGFR* mutations in IMA tumors. The frequency of *EGFR* mutations was positively correlated with PPA ($P = 0.00001$) and negatively correlated with SPA ($P = 0.00001$).

KRAS mutations were most prevalent in IMAs (74.4%), followed by MPAs (16.2%), PPAs (15.6%), LPAs (9.2%), SPAs (5.3%), AIS + MIAs (4.0%), and APAs (3.7%). The frequency of *KRAS* mutations was positively correlated with IMA ($P = 0.00001$).

ALK translocations were most prevalent in MPAs (15.0%), followed by APAs (14.4%), SPAs (6.5%), PPAs (2.4%) and IMA (2.2%). There were no *ALK* translocations in AIS + MIA or LPA ADCs. The frequency of *ALK* translocations was positively correlated with the MPA and APA tumor types ($P = 0.00001$ and 0.0002, respectively).

4. Discussion

The present study revealed that the IASLC/ATS/ERS classification of ADCs correlates with patient prognosis, provides appropriate diagnostic criteria for AIS and MIA, and confirms the importance of lymphovascular invasion as a prognostic factor for analyzing T1 tumor. In addition, this classification also predicts ADC subtypes with driver gene alterations, such as PPA for *EGFR* mutations, IMA for *KRAS* mutations, and APA and MPA for *ALK* translocations.

Although the classification we used was slightly different from the original IASLC/ATS/ERS classification [2], including the combination of AIS and MIA subtypes and special variants were consisted of only IMA, we revealed that the IASLC/ATS/ERS classification correlates with patient outcomes. The results also demonstrated that the previously used groupings [6], i.e., the dividing of ADCs into 3 group (AIS + MIA, LPA + APA + PPA, and MPA + SPA + other variants)

also predicted patient outcome in a meaningful manner. Traditional statistical tests for association, including likelihood ratio tests, cannot determine whether markers or models will be clinically useful for risk prediction [15]. Compared to these tests, the recently developed IDI has an improved risk discrimination resulting from the estimation of the differences in the mean predicted probabilities of the outcome between those with and without the outcome in question, after introducing the candidate biomarker to the model [16]. Thus, the results from the current study imply that subdividing ADCs into 7 groups is more meaningful, compared with the use of combined histological groupings, due to the higher IDI values observed after classifying ADCs into 7 groups (0.0175) than when they were divided into the combined histological grouping (0.0111).

As reported previously [6,9], both AIS and MIA demonstrated 100% disease-specific survival in the present series. Since the publication of the seminal article by Noguchi et al. [17], many authors have recognized favorable subsets of invasive ADC and have attempted to discriminate MIA from other invasive ADCs. Noguchi et al. reported that not only pure BAC, but also focally invasive tumors, without vascular or pleural invasions, showed 100% disease-free survival [17]. Suzuki et al. reported that the probability of pathologic lymph node involvement was low and that the outcome was excellent (5-year survival, 100%), if the lung ADC was ≤2.0 cm in size with central fibrosis of ≤5 mm [18]. As also described in the present report, MIA with scar sizes of ≤5 mm have been reported to show favorable outcomes [19–24]. Recently, another group reported a single case of tumor recurrence in a patient with MIA, as defined by the IASLC/ATS/ERS classification, but the authors did not perform the molecular analysis necessary to distinguish between recurrence and metachronous carcinoma [25]. In the present cohort, none of the 33 MIA patients demonstrated recurrence. Although close follow-up is needed for these patients, the current data validated the usefulness of the IASLC/ATS/ERS criteria for MIA for patient management.

Based on the above results, a separate analysis was undertaken to determine whether or not AIS + MIA tumors should be classified as T1 or Tis. There were statistical differences between AIS + MIA tumors and T1 tumors excluding AIS + MIA ($P < 0.0001$). Similar to squamous carcinoma in situ of the lung that is expected to be 100% curable, the current data suggest that AIS and MIA should be classified as Tis, as opposed to T1. However, a prospective study involving a larger number of cases will be required to confirm the appropriate classification of AIS and MIA.

The significance of lymphovascular invasion on OS was explored by analyzing the 506 T1 cases. The prognosis of T1 tumors, without lymphovascular invasion, was compared to that of T1 tumors with lymphovascular invasion. Similar to previous reports [26–29], patients with lymphovascular invasion had a worse prognosis than those without. The 5- and 10-year OS rates of T1 tumors, without lymphovascular invasion, was significantly longer than the OS rates for those tumors if lymphovascular invasion was present ($P = 0.0003$). Although, statistically marginal differences of the OS rates was observed between T1 tumors with lymphovascular invasion and T2a tumors ($P = 0.064$), survival curves of T1 tumors with lymphovascular invasion were clearly lower than T1 tumors ($P < 0.0001$). These data suggest that lung T1 ADCs with lymphovascular invasion may be better staged as T2a. Neither the current study nor previous reports examining vascular invasion discriminated between pulmonary artery and venous blood vessel invasion as a significant prognostic indicator. Considering the hemodynamics, pulmonary artery invasion would not be expected to affect prognosis, but the results may indicate that blood vessel invasion reflects the destructive ability of the tumor [30]. Incorporating lymphovascular status into staging is already in practice for testicular non-seminomatous germ cell tumors, where lymphovascular invasion confers an approximately 50% likelihood of retroperitoneal metastasis; T1 tumors with lymphovascular invasion have been, therefore, reclassified as T2 tumors [31].

The IASLC/ATS/ERS classification system was also found to correlate with observations of gene alterations (*EGFR*, *KRAS*, and *ALK*). These driver gene alterations were mutually exclusive. There was a positive correlation between *EGFR* mutations and PPA and a negative correlation between *EGFR* mutations and SPA. Before the IASLC/ATS/ERS classification, most studies revealed the correlation between *EGFR* mutations and papillary histology [3,32]. On the basis of the IASLC/ATS/ERS classification, Shim et al. reported a positive association between *EGFR* mutations and MPA [33]. However, the cohort of their report was only 120 cases of ADC and did not analyze other driver mutations. On the other hand, Zhang and colleagues reported a positive association between *EGFR* mutations and APA [34].

Consistent with previous reports [34–36], IMA was the subtype most associated with a higher prevalence of *KRAS* mutations. There were no *ALK* translocations in cases of AIS, MIA, or LPA. The frequency of *ALK* translocations was, however, positively correlated with MPA and APA. The histological features of lung cancers with *ALK* translocations are more likely to demonstrate ADCs with a mucinous cribriform pattern where the pattern is representative of the acinar component and/or a solid growth pattern containing signet ring cells [12,37]. A previous report analyzing *ALK*-translocated ADCs, based on the IASLC/ATS/ERS classification, revealed that MPAs, SPAs, or PPAs were independently associated with *ALK* translocations [38]. However, Zhang et al. [34] reported that APA was correlated with *EGFR* mutations, as described above. This discordance may be due to the differences in the criteria of each observer [39]. Recent study revealed that discussions and training might overcome insecurities on how to classify and increase the congruence [40].

In conclusion, the IASLC/ATS/ERS classification that separates ADCs into 7 subtypes not only predicts prognosis, but also provides a subtype association with specific driver-gene alterations. However there were statistical differences been IASLC/ATS/ERS classification and these driver gene alterations, other than IMA for *KRAS* mutations, *EGFR* mutations were detected 30–56% in several other subtypes and *ALK* rearrangements were detected at most 15%. Our results also suggest that AIS and MIA should be reclassified as Tis and that the T1 tumors with lymphovascular invasion may be better staged as T2a, based on survival data.

Financial support

This work was supported in part by the National Cancer Center Research and Development Fund (23-A-2), (23-A-11), and (23-A-35).

Conflict of interest

None of the authors has any conflict of interest.

Acknowledgements

We would like to thank Susumu Wakai, Karin Yokozawa, Shoko Nakamura, and Ryousuke Yamaga for their skillful technical assistance.

References

[1] Travis WD, Brambllla E, Muller-Hermelink HK, Harris CC. Pathology and genetics of tumors of the lung, pleura, thymus and heart. Lyon (France): IARC Press; 2004.
[2] Travis WD, Brambilla E, Noguchi M, Nicholson AG, Geisinger KR, Yatabe Y, et al. International Association for the Study of Lung Cancer/American Thoracic

Society/European Respiratory Society International Multidisciplinary Classification of lung adenocarcinoma. J Thorac Oncol 2011;6:244–85.
[3] Motoi N, Szoke J, Riely GJ, Seshan VE, Kris MG, Rusch VW, et al. Lung adenocarcinoma: modification of the 2004 WHO mixed subtype to include the major histologic subtype suggests correlations between papillary and micropapillary adenocarcinoma subtypes, EGFR mutations and gene expression analysis. Am J Surg Pathol 2008;32:810–27.
[4] Pao W, Miller V, Zakowski M, Doherty J, Politi K, Sarkaria I, et al. EGF receptor gene mutations are common in lung cancers from "never smokers" and are associated with sensitivity of tumors to gefitinib and erlotinib. Proc Natl Acad Sci U S A 2004;101:13306–11.
[5] Kim YH, Ishii G, Goto K, Nagai K, Tsuta K, Shiono S, et al. Dominant papillary subtype is a significant predictor of the response to gefitinib in adenocarcinoma of the lung. Clin Cancer Res 2004;10:7311–7.
[6] Yoshizawa A, Motoi N, Riely GJ, Sima CS, Gerald WL, Kris MG, et al. Impact of proposed IASLC/ATS/ERS classification of lung adenocarcinoma: prognostic subgroups and implications for further revision of staging based on analysis of 514 stage I cases. Mod Pathol 2011;24:653–64.
[7] Russell PA, Wainer Z, Wright GM, Daniels M, Conron M, Williams RA. Does lung adenocarcinoma subtype predict patient survival?: A clinicopathologic study based on the new International Association for the Study of Lung Cancer/American Thoracic Society/European Respiratory Society international multidisciplinary lung adenocarcinoma classification. J Thorac Oncol 2011;6:1496–504.
[8] Warth A, Muley T, Meister M, Stenzinger A, Thomas M, Schirmacher P, et al. The novel histologic International Association for the Study of Lung Cancer/American Thoracic Society/European Respiratory Society classification system of lung adenocarcinoma is a stage-independent predictor of survival. J Clin Oncol 2012;30:1438–46.
[9] Gu J, Lu C, Guo J, Chen L, Chu Y, Ji Y, et al. Prognostic significance of the IASLC/ATS/ERS classification in Chinese patients—a single institution retrospective study of 292 lung adenocarcinoma. J Surg Oncol 2012;107:474–80.
[10] Goldstraw P. International Association for the Study of Lung Cancer Staging Manual in Thoracic Oncology. 2009.
[11] Takano T, Ohe Y, Tsuta K, Fukui T, Sakamoto H, Yoshida T, et al. Epidermal growth factor receptor mutation detection using high-resolution melting analysis predicts outcomes in patients with advanced non small cell lung cancer treated with gefitinib. Clin Cancer Res 2007;13:5385–90.
[12] Yoshida A, Tsuta K, Nitta H, Hatanaka Y, Asamura H, Sekine I, et al. Bright-field dual-color chromogenic in situ hybridization for diagnosing echinoderm microtubule-associated protein-like 4-anaplastic lymphoma kinase-positive lung adenocarcinomas. J Thorac Oncol 2011;6:1677–86.
[13] Pencina MJ, D'Agostino RB, Steyerberg EW. Extensions of net reclassification improvement calculations to measure usefulness of new biomarkers. Stat Med 2011;30:11–21.
[14] R Development Core Team. A language and environment for statistical computing. Vienna, Austria: R Foundation for Statistical Computing; 2011, ISBN 3-900051-07-0 http://www.R-project.org/
[15] Pepe MS, Janes H, Longton G, Leisenring W, Newcomb P. Limitations of the odds ratio in gauging the performance of a diagnostic, prognostic, or screening marker. Am J Epidemiol 2004;159:882–90.
[16] Cook NR, Paynter NP. Performance of reclassification statistics in comparing risk prediction models. Biom J 2011;53:237–58.
[17] Noguchi M, Morikawa A, Kawasaki M, Matsuno Y, Yamada T, Hirohashi S, et al. Small adenocarcinoma of the lung. Histologic characteristics and prognosis. Cancer 1995;75:2844–52.
[18] Suzuki K, Yokose T, Yoshida J, Nishimura M, Takahashi K, Nagai K, et al. Prognostic significance of the size of central fibrosis in peripheral adenocarcinoma of the lung. Ann Thorac Surg 2000;69:893–7.
[19] Daly RC, Trastek VF, Pairolero PC, Murtaugh PA, Huang MS, Allen MS, et al. Bronchoalveolar carcinoma: factors affecting survival. Ann Thorac Surg 1991;51:368–76 [discussion 76-7].
[20] Garfield DH, Cadranel J, West HL. Bronchioloalveolar carcinoma: the case for two diseases. Clin Lung Cancer 2008;9:24–9.
[21] Kurokawa T, Matsuno Y, Noguchi M, Mizuno S, Shimosato Y. Surgically curable "early" adenocarcinoma in the periphery of the lung. Am J Surg Pathol 1994;18:431–8.
[22] Borczuk AC, Qian F, Kazeros A, Eleazar J, Assaad A, Sonett JR, et al. Invasive size is an independent predictor of survival in pulmonary adenocarcinoma. Am J Surg Pathol 2009;33:462–9.
[23] Kim EA, Johkoh T, Lee KS, Han J, Fujimoto K, Sadohara J, et al. Quantification of ground-glass opacity on high-resolution CT of small peripheral adenocarcinoma of the lung: pathologic and prognostic implications. AJR Am J Roentgenol 2001;177:1417–22.
[24] Lin DM, Ma Y, Zheng S, Liu XY, Zou SM, Wei WQ. Prognostic value of bronchioloalveolar carcinoma component in lung adenocarcinoma. Histol Histopathol 2006;21:627–32.
[25] Xu L, Tavora F, Battafarano R, Burke A. Adenocarcinomas with prominent lepidic spread: retrospective review applying new classification of the American Thoracic Society. Am J Surg Pathol 2012;36:273–82.
[26] Funai K, Sugimura H, Morita T, Shundo Y, Shimizu K, Shiiya N. Lymphatic vessel invasion is a significant prognostic indicator in stage IA lung adenocarcinoma. Ann Surg Oncol 2011;18:2968–72.
[27] Yokose T, Suzuki K, Nagai K, Nishiwaki Y, Sasaki S, Ochiai A. Favorable and unfavorable morphological prognostic factors in peripheral adenocarcinoma of the lung 3 cm or less in diameter. Lung Cancer 2000;29:179–88.
[28] Shimada Y, Saji H, Yoshida K, Kakihana M, Honda H, Nomura M, et al. Pathological vascular invasion and tumor differentiation predict cancer recurrence in stage is non-small-cell lung cancer after complete surgical resection. J Thorac Oncol 2012;7:1263–70.
[29] Brechot JM, Chevret S, Charpentier MC, Appere de Vecchi C, Capron F, Prudent J, et al. Blood vessel and lymphatic vessel invasion in resected nonsmall cell lung carcinoma. Correlation with TNM stage and disease free and overall survival. Cancer 1996;78:2111–8.
[30] Fujita A, Kameda Y, Goya T. Clinicopathology of stromal invasion in lung adenocarcinoma. Pathol Int 2009;59:1–6.
[31] Bosl GJ, Bajorin D, Sheinfeld J, Motzer R. Cancer of the testis. In: Devita VT, Hellman S, Rosenberg S, editors. Cancer: principles and practice of oncology. 5th ed. Philadelphia: J.B. Lippincott; 1977. p. 1397–425.
[32] Takano T, Ohe Y, Sakamoto H, Tsuta K, Matsuno Y, Tateishi U, et al. Epidermal growth factor receptor gene mutations and increased copy numbers predict gefitinib sensitivity in patients with recurrent non-small-cell lung cancer. J Clin Oncol 2005;23:6829–37.
[33] Shim HS, Lee da H, Park EJ, Kim SH. Histopathologic characteristics of lung adenocarcinomas with epidermal growth factor receptor mutations in the International Association for the Study of Lung Cancer/American Thoracic Society/European Respiratory Society lung adenocarcinoma classification. Arch Pathol Lab Med 2011;135:1329–34.
[34] Zhang Y, Sun Y, Pan Y, Li C, Shen L, Li Y, et al. Frequency of driver mutations in lung adenocarcinoma from female never-smokers varies with histologic subtypes and age at diagnosis. Clin Cancer Res 2012;18:1947–53.
[35] Marchetti A, Buttitta F, Pellegrini S, Chella A, Bertacca G, Filardo A, et al. Bronchioloalveolar lung carcinomas: K-ras mutations are constant events in the mucinous subtype. J Pathol 1996;179:254–9.
[36] Finberg KE, Sequist LV, Joshi VA, Muzikansky A, Miller JM, Han M, et al. Mucinous differentiation correlates with absence of EGFR mutation and presence of KRAS mutation in lung adenocarcinomas with bronchioloalveolar features. J Mol Diagn 2007;9:320–6.
[37] Takeuchi K, Choi YL, Togashi Y, Soda M, Hatano S, Inamura K, et al. KIF5B-ALK, a novel fusion oncokinase identified by an immunohistochemistry-based diagnostic system for ALK-positive lung cancer. Clin Cancer Res 2009;15:3143–9.
[38] Nishino M, Klepeis VE, Yeap BY, Bergethon K, Morales-Oyarvide V, Dias-Santagata D, et al. Histologic and cytomorphologic features of ALK-rearranged lung adenocarcinomas. Mod Pathol 2012.
[39] Thunnissen E, Beasley MB, Borczuk AC, Brambilla E, Chirieac LR, Dacic S, et al. Reproducibility of histopathological subtypes and invasion in pulmonary adenocarcinoma. An international interobserver study. Mod Pathol 2012;25:1574–83.
[40] Warth A, Cortis J, Fink L, Fisseler-Eckhoff A, Geddert H, Hager T, et al. Training increases concordance in classifying pulmonary adenocarcinomas according to the novel IASLC/ATS/ERS classification. Virchows Arch 2012;461:185–93.

Human Pathology (2013) 44, 2636–2642

ELSEVIER

Human
PATHOLOGY

www.elsevier.com/locate/humpath

Original contribution

Distinct clinicopathologic characteristics of lung mucinous adenocarcinoma with *KRAS* mutation☆

Hideomi Ichinokawa MD, PhD[a,b,c], Genichiro Ishii MD, PhD[a,*], Kanji Nagai MD, PhD[b], Akikazu Kawase MD, PhD[b], Junji Yoshida MD, PhD[b], Mitsuyo Nishimura MD, PhD[b], Tomoyuki Hishida MD, PhD[b], Naomi Ogasawara BS[c], Katsuya Tsuchihara MD, PhD[c], Atsushi Ochiai MD, PhD[a,*]

[a]*Pathology Division, Research Center for Innovative Oncology, National Cancer Center Hospital East, Kashiwa, 277-8577 Chiba, Japan*
[b]*Division of Thoracic Oncology, National Cancer Center Hospital East, Kashiwa, 277-8577 Chiba, Japan*
[c]*Cancer Physiology Project, Research Center for Innovative Oncology, National Cancer Center Hospital East, Kashiwa, 277-8577 Chiba, Japan*

Received 3 January 2013; revised 13 May 2013; accepted 17 May 2013

Keywords:
Epidermal growth factor receptor (*EGFR*);
KRAS;
Mucinous adenocarcinoma

Summary Primary mucinous adenocarcinomas are uncommon, and their pathogenesis remains unclear. We recently reported the clinicopathologic characteristics of surgically resected mucinous adenocarcinoma, including the frequent involvement of the left and lower lung and absence of central fibrosis. The present study attempted to clarify the pathogenesis of mucinous adenocarcinoma based on *KRAS* mutation status. We selected 45 mucinous adenocarcinoma cases from among 2474 surgically resected primary lung adenocarcinomas. Of these, 22 had a *KRAS* mutation (48.9%), whereas only 7 (15.6%) had an *epidermal growth factor receptor* mutation, and 2 cases had both mutations. The mucinous adenocarcinomas with *KRAS* mutations were located in the lower lung lobe significantly more often ($P < .05$) than were tumors without *KRAS* mutation. The mucinous adenocarcinoma cases with *KRAS* mutations also had a significantly lower frequency of nuclear atypia ($P < .05$). We compared the degree of immunostaining for matrix metalloproteinase-7 (MMP-7), laminin-5, and geminin in the mucinous adenocarcinoma with and without *KRAS* mutation. The proportion of geminin-positive cells was lower among the cases with a mutation than among those without (0.7% versus 2.1%; $P < .05$). No significant differences in the extent of staining of the other markers were observed between the groups. The current study clearly demonstrated that mucinous adenocarcinomas with *KRAS* mutations have clinicopathologic characteristics different from those of mucinous adenocarcinoma without such mutations.

1. Introduction

Lung adenocarcinomas are characterized by a high degree of morphologic heterogeneity. With reference to the cytologic features of the cells, Shimosato et al [1] and Kimula [2] subclassified primary tumor cells into 5 subgroups: goblet, bronchial cell surface type, bronchial gland, Clara, and type II

☆ Conflict of interest: The authors have declared no conflicts of interest.

* Corresponding author. Pathology Division, Research Center for Innovative Oncology, National Cancer Center Hospital East 6-5-1, Kashiwanoha, Kashiwa Chiba 277-8577, Japan.
E-mail addresses: gishii@east.ncc.go.jp (G. Ishii), aochiai@east.ncc.go.jp (A. Ochiai).

0046-8177/$ – see front matter © 2013 Elsevier Inc. All rights reserved.
http://dx.doi.org/10.1016/j.humpath.2013.05.026

pneumocyte. In recent years, lung adenocarcinoma composed predominantly of goblet cells has been classified as mucinous adenocarcinoma (MA) [3]. Previous authors have reported that MA is less frequently associated with lymph node metastasis than other adenocarcinomas but is associated with lobar pneumonic clinical features [4]. Wislez et al [5] reported that MA appears to be resistant to epidermal growth factor receptor (EGFR)–tyrosine kinase inhibitors (TKIs). On the other hand, they may be more sensitive to taxane [6,7].

Malignant neoplasms are considered to develop through the accumulation of genetic abnormalities. In lung cancer, *KRAS* and *EGFR* mutations frequently are detected. *KRAS* mutation is the most common driver mutation in human cancers, although the prevalence of mutations and the affected codons differ according to the type of cancer. In lung adenocarcinoma, the frequency of *KRAS* mutation–positive cases is 5% to 40%, and mutations are more common in male patients and in smokers [8-12]. On the other hand, *EGFR* mutation has been an area of particular interest because of the finding that the administration of EGFR-TKIs in clinical trials resulted in a high response rate among patients with lung adenocarcinoma carrying an *EGFR* mutation. These mutations were correlated with the observed clinical characteristics of responders to TKIs, including female sex, Asian ethnicity, an absent or infrequent smoking history, and a diagnosis of lung adenocarcinoma [13-15]. Furthermore, mutations in *KRAS* and *EGFR* usually are mutually exclusive.

We recently reported that the clinicopathologic characteristics of MA include the frequent involvement of the left and lower lung and absence of central fibrosis [4]; these adenocarcinomas form a distinct subset and should be considered different from other lung adenocarcinomas. The present study attempted to clarify the pathogenesis of MA with special reference to *KRAS* and *EGFR* mutation status. We analyzed the correlations between the mutations and clinicopathologic characteristics.

2. Materials and methods

2.1. Patients

Between August 1992 and March 2010, a total of 2474 patients with primary adenocarcinoma of the lung were treated surgically in the Division of Surgery of the Department of Thoracic Oncology, National Cancer Center Hospital East, Chiba, Japan. From these, 45 MAs (2.1%) were selected for study. The data collection and analyses were approved by the institutional review board, and the need to obtain informed consent from each patient was waived.

2.2. Clinical information

All available clinical information was obtained from the clinical records and reports completed by the referring physicians. The records were reviewed for patient age; sex; smoking index; and tumor size, stage, and location.

2.3. Pathologic information

The resected tissues had been fixed in 10% formalin or absolute methyl alcohol and embedded in paraffin. Serial 4-μm sections were stained with hematoxylin and eosin using the Alcian blue–periodic acid Schiff method to visualize cytoplasmic mucin production or the Victoria van Gieson method to identify elastic fibers. The tumors were classified according to the criteria of the current histologic classification adopted by the World Health Organization [16]. Tumor cells of MA have a goblet or columnar morphology with abundant intracytoplasmic mucin. The apex of each cell typically is occupied by a large mass of mucin, and the carcinoma cells show mucin production with mucus pooling in the surrounding alveolar spaces. [3,17-20].

The 45 MAs examined in this study were classified into 3 groups: mucinous adenocarcinoma in situ (size $\leq$3 cm; n = 24), mucinous minimally invasive adenocarcinoma (size $\leq$3 cm; n = 1), and invasive mucinous adenocarcinoma (size >3 cm; n = 20). Nuclear atypia was said to be present when there was nuclear enlargement, prominent nucleoli, or overlapping nuclei (Fig. 1). Pathologic staging was performed according to the classification of the Union for International Cancer Control [21].

2.4. Antibodies and immunohistochemical staining

Immunohistochemical staining was performed according to the method previously reported [22]. We used 3 antibodies: laminin-5 subunit γ2 (clone D4B5; Chemicon, Temecula, CA), MMP-7 (matrilysin, clone 141-7B2; Daiichi Fine Chemical, Toyama, Japan), and geminin (clone EM6; Novocastra, Newcastle-upon-Tyne, UK). We used the immunohistochemical status of laminin-5, MMP-7, and geminin to evaluate the proliferative ability and invasive capacity of the cancer cells. Basement membranes of bronchial epithelium, lymphocytes in germinal centers, and human lung adenocarcinomas were used as positive controls for laminin-5, geminin, and MMP-7, respectively. As the negative control, we added diluent containing 10% swine serum and confirmed that no nonspecific reaction was shown.

2.5. Staining scores

All the stained tissue sections were scored semiquantitatively and evaluated independently under a light microscope by 2 observers (H. I. and G. I.) with no knowledge of the clinicopathologic data. When the evaluations differed, the tissues were examined by both observers through a multiheaded conference microscope, and a consensus was reached. The labeling scores, except for geminin, were calculated by multiplying the percentage of stained tumor cells per lesion (0%-100%) by the staining intensity (0,

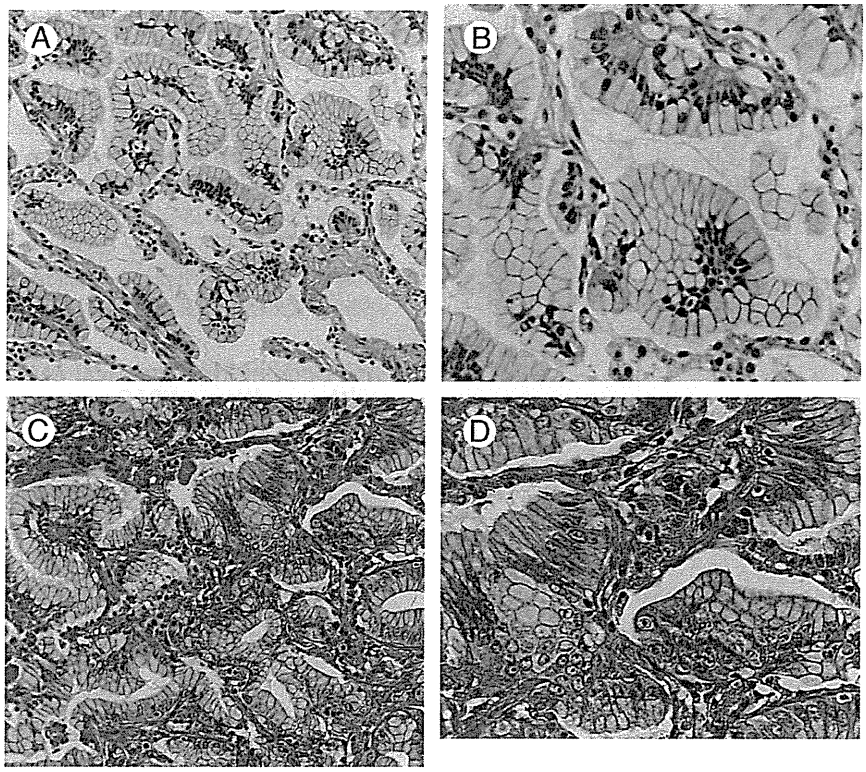

Fig. 1 Typical morphology of MA, characterized by tall columnar cells with basal nuclei and pale cytoplasm and various amounts of cytoplasmic mucin. Apex of each cell is occupied by large mass of mucus, which compresses nucleus toward basal end of the cell. A and B, Tumors with *KRAS* mutation: nuclear enlargement, prominent nucleoli, and overlapping nuclei are rarely observed (A, ×10; B, ×40). C and D, Tumors without *KRAS* mutation: nuclear enlargement, prominent nucleoli, and overlapping nuclei are visible (C, ×10; D, ×40).

negative; 1, weak; 2, strong), with the resulting possible scores ranging from 0 to 200. In the case of geminin, the number of positively stained cells per 1000 tumor cells was counted. Two independent observers' average was assigned as the staining score for each case. The weighted κ statistics for laminin-5, MMP-7, and geminin were 0.701, 0.734, and 0.842, respectively.

2.6. *KRAS* and *EGFR* mutation analysis

We isolated DNA from formalin-fixed, paraffin-embedded surgical specimens. The tumor samples were mapped using hematoxylin and eosin staining and manually macrodissected with a needle, and genomic DNA was isolated using the QIAamp DNA FFPE Tissue Kit (Qiagen, Venlo, The Netherlands). The *KRAS* mutation in codons 12 and 13 of the exon 2 fragment was amplified according to a previously described method [9-11,23,24]. The *EGFR* exons 18 to 21 were amplified largely according to a previously described method [10,24-26].

2.7. Statistical analysis

The Fisher exact probability test was used to compare binomial proportions. The Mann-Whitney *U* test was used to compare the staining scores. $P < .05$ was considered statistically significant. All the statistical analyses were performed using SPSS version 11.0 (SPSS, Inc, Chicago, IL).

3. Results

3.1. Clinicopathologic findings

The clinicopathologic data for the MA cases are summarized in Table 1. Of the 45 patients, 19 were men and 26 were women, and 17 of the patients (38%) were smokers (smoking index ≥200; 13 men, 4 women). The maximum diameters of the tumors ranged from 0.7 to 19.5 cm. Pleural invasion was observed in 1 case (2%). Lymphatic invasion likewise was present in 1 case. Pulmonary metastasis and vascular invasion were not observed.

3.2. *KRAS* and *EGFR* mutational analysis

The *KRAS* and *EGFR* mutational status of the 45 MA cases is shown in Table 2. *KRAS* mutation was identified in 22 cases (49%). The most frequent mutation was G12V (14 patients), followed by G12C (5 patients), and G12D (3

Table 1 Clinicopathologic data of 45 mucinous adenocarcinomas

Parameter	n (%)
Age (y)	
<65	19 (42)
≥65	26 (58)
Sex	
Male	19 (42)
Female	26 (58)
Smoking index	
<200	28 (62)
≥200	17 (38)
Tumor size (cm)	
≤3	30 (67)
>3	15 (33)
Location	
Right	20 (44)
Left	25 (56)
Lobe	
Upper/middle	10 (22)
Lower	35 (78)
Pathologic T stage	
1	30 (67)
2-4	15 (33)
Pathologic N stage	
0	45 (100)
1-3	0
Pathologic stage	
1	39 (87)
2-4	6 (13)
Pleural invasion	1 (2)
Pulmonary metastasis	0
Lymphatic permeation	1 (2)
Vascular invasion	0
Nuclear atypia	20 (44)
Central fibrosis	7 (16)

patients). No mutation in codon 13 was found. Mutations of *EGFR* were identified in 7 cases (16%). All were detected in exon 21 (L858R). That is, mutations in exons 19, 20, and 22 were not found. Two patients had concomitant *KRAS* and *EGFR* mutations. The specific mutations were a *KRAS* mutation at codon 12 (G12V) and an *EGFR* mutation within exon 21 (L858R). A case with pleural invasion exhibited *KRAS* mutation G12C. A case with lymphatic permeation did not exhibit either *KRAS* or *EGFR* mutation.

Table 2 *KRAS* and *EGFR* status of 45 mucinous adenocarcinomas

Gene	Mutation	n (%)
KRAS	G12V	14 (64)
	G12C	5 (23)
	G12D	3 (13)
	None	23
EGFR	L858R	7 (100)
	None	38

3.3. Clinicopathologic comparison of MA cases with or without *KRAS* mutation

The MA cases with *KRAS* mutation were significantly more likely to be located in the lower pulmonary lobe ($P < .05$) than were tumors without the mutation (Table 3). The tumors with *KRAS* mutation (Fig. 1A and B) showed significantly less nuclear atypia (enlargement, prominent nucleoli, and overlapping nuclei) ($P < .05$) than cases without *KRAS* mutation (Fig. 1C and D).

3.4. Immunohistochemical comparison of MA cases with or without *KRAS* mutation

Because nuclear atypia is a feature of malignancy, we assumed that the proliferation ability and the invasive capacity of MA cases with and without *KRAS* mutation

Table 3 Relation between *KRAS* mutation and mucinous adenocarcinoma features

	KRAS mutation (%)		*P*
	Negative (n = 23)	Positive (n = 22)	
Age (y)			.18
<65	12 (52)	7 (32)	
≥65	11 (48)	15 (68)	
Sex			.87
Male	10 (43)	9 (41)	
Female	13 (57)	13 (59)	
Smoking index			.68
<200	15 (65)	13 (59)	
≥200	8 (35)	9 (41)	
Tumor size (cm)			.84
≤3	15 (65)	15 (68)	
>3	8 (35)	7 (32)	
Location			.297
Right	12 (52)	8 (36)	
Left	11 (48)	14 (64)	
Lobe			.0083
Upper/middle	8 (35)	2 (9)	
Lower	15 (65)	20 (91)	
Pathologic T stage			.84
1	15 (65)	15 (68)	
2-4	8 (35)	7 (32)	
Pathologic N stage			1
0	23 (100)	22 (100)	
1-3	0	0	
Pathologic stage			.67
1	19 (83)	20 (91)	
2-4	4 (17)	2 (9)	
Pleural invasion	0	1 (5)	.31
Pulmonary metastasis	0	0	1
Lymphatic permeation	1 (4)	0	.33
Vascular invasion	0 (0)	0 (0)	1
Nuclear atypia	15 (65)	5 (23)	.0034
Central fibrosis	5 (22)	2 (9)	.25

Table 4 Relation between *KRAS* mutation and marker expression

	KRAS mutation		*P*
	Negative (n = 23)	Positive (n = 22)	
Laminin			.27
Mean	7.6	5.5	
Range	0-50	0-50	
MMP-7			.35
Mean	27	20	
Range	0-80	0-50	
Geminin			.003
Mean	2.1	0.69	
Range	0.25-7.42	0.16-2.44	

were different. Laminin-5 and MMP-7 expressions are reported to be associated with invasive capacity of tumor cells, whereas geminin expression is closely associated with proliferation (Table 4). The mean staining scores for laminin-5 in the MA cases with and without *KRAS* mutation were 5.5 and 7.6, respectively. The mean staining scores for MMP-7 cases and those without *KRAS* mutation were 19.5 and 27.0, respectively. There were no significant differences in the expression of laminin-5 or MMP-7 in the 2 groups. The mean positive rates for geminin in the MA cases with and without *KRAS* mutation were 0.7 and 2.1, respectively. The positive rate for geminin in the MA cases with *KRAS* mutation was significantly lower than that in cases without *KRAS* mutation ($P < .05$; Fig. 2).

4. Discussion

This is the first report of the relation between *KRAS* mutation status and the clinicopathologic features of MA. The tumors with *KRAS* mutation were significantly more likely to be located in the lower lobe ($P < .05$) than tumors without *KRAS* mutation. The MA cases with *KRAS* mutations also showed a significantly lower frequency of nuclear atypia ($P < .05$) than cases without. Moreover, the proportion of cells in the S, G_2, and M phases (geminin-positive cells) among the cases with *KRAS* mutation was significantly lower than among the cases without a mutation ($P < .05$). Therefore, the pathogenesis of MA may be classifiable into 2 groups according to *KRAS* mutation status.

In general, activated *KRAS* enhances cell proliferation. In lung tumors, *KRAS* mutations are thought to occur early in the genesis of adenocarcinomas, as they are found in 25% to 35% of atypical adenomatous hyperplasia, the precursor of certain types of adenocarcinomas [27,28]. On the other hand, Okudela et al [29,30] demonstrated that the forced expression of oncogenic *KRAS* induced severe growth suppression in immortalized human airway epithelial cells. Although the above findings were based on in vitro observations, these results might explain our current report in that the positive rate for geminin in MA cases with *KRAS* mutation was significantly lower than that in cases without *KRAS* mutation.

Type 1 congenital cystic adenomatoid malformations (CCAMs) are composed of one or more cysts greater than 2 cm in diameter surrounded by often underdeveloped alveolar parenchyma and a variable number of smaller cysts. In approximately one-third of cases, papillary tufts of cytologically bland mucinous cells punctuate the cyst surface [31,32]. Lantuejoul et al [33] suggested that mucinous cells in type 1 CCAM may represent mucinous bronchioloalveolar carcinoma (BAC) precursors. In mucinous cell clusters associated with CCAM, *KRAS* mutations

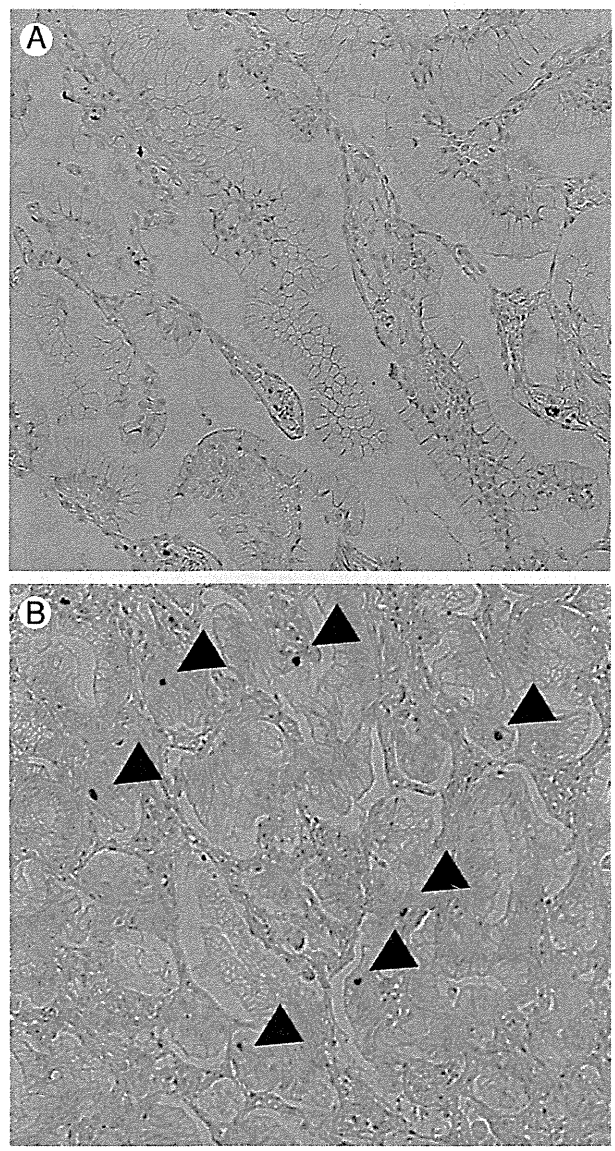

Fig. 2 Immunostaining for geminin in MA with different *KRAS* mutation status (×10). A, Tumor with *KRAS* mutation: geminin-positive rate is 0. B, Tumor without *KRAS* mutation: scattered geminin-positive cells (arrowheads) are visible (positive rate, 9.0).

were detected in 5 of 6 cases, whereas no *EGFR* mutations were reported. Furthermore, all mucinous cell cluster lesions displayed a staining pattern similar to that of mucinous BAC. These findings suggested that type 1 CCAM mucinous cells represent mucinous BAC precursors. Actually, CCAM also exhibits greater likelihood of being located in the lower lobe, similar to MA with a *KRAS* mutation in the current study. Among our 45 cases, however, no findings similar to those of CCAM were seen in the noncancerous fields. Further examination is needed to determine the relation between the pathogenesis of CCAM and of MA with a *KRAS* mutation.

Mutations of *KRAS* and *EGFR* in lung adenocarcinoma are reportedly found in a mutually exclusive manner [15,24,34]. However, a few cases with double mutations have been described. Among the 45 lesions in the present series, 2 had concomitant *EGFR* and *KRAS* mutations. These 2 cases displayed a *KRAS* mutation at codon 12 (G12V) and an *EGFR* mutation within exon 21 (L858R). The 2 cases did not have any clinical features in common.

Mutations of *EGFR* were identified in 7 (16%) of the 45 MA cases. No distant recurrences were observed in the 7 cases with these mutations. Of the 7 patients, 2 were men and 5 were women (male/female ratio, 1:2.5). Two of the patients (29%), both men, were smokers (smoking index $\geq$200). Compared with the MA cases without an *EGFR* mutation, the proportions of females and nonsmoker status were higher. Although the number of cases was limited, it appears that MA with *EGFR* mutation exhibits clinicopathologic characteristics similar to those of general primary lung adenocarcinomas.

In the current study, lower lobe location, a lesser frequency of nuclear atypia, and a smaller proportion of geminin-positive cells were characteristic features of MAs with *KRAS* mutations. However, they might be general characteristics of lung adenocarcinoma with this mutation. To rule out this possibility, it would be important to examine the clinicopathology of non-MA with *KRAS* mutation in the resectable cases.

In conclusion, we found that MAs with *KRAS* mutations exhibit different clinicopathologic characteristics than MAs without such mutations. Although further studies involving a larger number of cases are warranted, we believe that MA of the lung could be subclassified into distinct subtypes with different modes of pathogenesis according to *KRAS* mutation status.

Acknowledgments

This work was supported in part by a Grant-in-Aid for Cancer Research (19-10) from the Ministry of Health, Labor and Welfare, a Grant for Scientific Research Expenses for Health Labor and Welfare Programs, the Foundation for the Promotion of Cancer Research, 3rd-Term Comprehensive 10-year Strategy for Cancer Control, and Special Coordination Funds for Promoting Science and Technology from the Ministry of Education, Culture, Sports, Science and Technology of the Japanese Government.

References

[1] Shimosato Y, Kodama T, Kameya T. Morphogenesis of peripheral type adenocarcinoma of the lung. In: Shimosato Y, Melamed MR, Nettesheim P, editors. Morphogenesis of Lung Cancer, Vol. 1. Boca Raton: CRC Press; 1982. p. 65-89.

[2] Kimula Y. A histochemical and ultrastructural study of adenocarcinoma of the lung. Am J Surg Pathol 1978;2:253-64.

[3] Travis WD, Brambilla E, Noguchi M, et al. International Association for the Study of Lung Cancer/American Thoracic Society/European Respiratory Society International Multidisciplinary Classification of Lung Adenocarcinoma. J Thorac Oncol 2011;6:244-85.

[4] Ichinokawa H, Ishii G, Nagai K, et al. Clinicopathological characteristics of primary lung adenocarcinoma predominantly composed of goblet cells in surgically resected cases. Pathol Int 2011;6:423-9.

[5] Wislez M, Antoine M, Baudrin L, et al. Non-mucinous and mucinous subtypes of adenocarcinoma with bronchioloalveolar carcinoma features differ by biomarker expression and in the response to gefitinib. Lung Cancer 2010;68:185-91.

[6] Cadranel J, Quoix E, Baudrin L, et al. IFCT-0401 Trial: a phase II study of gefitinib administered as first-line treatment in advanced adenocarcinoma with bronchioloalveolar carcinoma subtype. J Thorac Oncol 2009;4:1126-35.

[7] West HL, Crowley JJ, Vance RB, et al. Advanced bronchioloalveolar carcinoma: a phase II trial of paclitaxel by 96 hour infusion (SWOG 9714): a Southwest Oncology Group Study. Ann Oncol 2005;16: 1076-80.

[8] Kobayashi T, Tsuda H, Noguchi M, et al. Association of point mutation in c-Ki-ras oncogene in lung adenocarcinoma with particular reference to cytologic subtypes. Cancer 1990;66:289-94.

[9] Riely GJ, Marks J, Pai W. *KRAS* mutations in non-small cell lung cancer. Proc Am Thorac Soc 2009;6:201-5.

[10] Sakuma Y, Matsukuma S, Yoshihara M, et al. Distinctive evaluation of nonmucinous and mucinous subtypes of bronchioloalveolar carcinoma in *EGFR* and *KRAS* gene-mutation analyses for Japanese lung adenocarcinomas: confirmation of the correlations with histologic subtypes and gene mutations. Am J Clin Pathol 2007;128:100-8.

[11] Suzuki M, Shigematsu H, Iizaka T, et al. Exclusive mutation in epidermal growth factor receptor gene, HER-2 and KRAS, and synchronous methylation of non-small cell lung cancer. Cancer 2006;106:2200-7.

[12] Tam IY, Chung LP, Suen WS, et al. Distinct epidermal growth factor receptor and *KRAS* mutation patterns in non-small cell lung cancer patients with different tobacco exposure and clinicopathologic features. Clin Cancer Res 2006;12:1647-53.

[13] Pham D, Kris MG, Riely GJ, et al. Use of cigarette-smoking history to estimate the likelihood of mutations in epidermal growth factor receptor gene exons 19 and 21 in lung adenocarcinomas. J Clin Oncol 2006;24:1700-4.

[14] Miller VA, Kris MG, Shah N, et al. Bronchioloalveolar pathologic subtype and smoking history predict sensitivity to gefitinib in advanced non-small cell lung cancer. J Clin Oncol 2004;22:1103-9.

[15] Marchetti A, Martella C, Felicioni L, et al. *EGFR* mutations in non-small-cell lung cancer: analysis of a large series of cases and development of a rapid and sensitive method for diagnostic screening with potential implications on pharmacologic treatment. J Clin Oncol 2005;23:857-65.

[16] Travis WD, Brambilla E, Muller-Hermelink HK, Harris CC. WHO Classification of Tumors. Pathology and Genetics of Tumors of the Lung, Pleura, Thymus and Heart. Lyon: IARC Press; 2004.

[17] Colby TV, Koss MN, Travis WD. Tumors of the Lower Respiratory Tract. Atlas of Tumor Pathology. Vol. 3. Washington DC: Armed Forces Institute of, Pathology; 1995. p. 203–34.
[18] Travis WD, Colby TV, Corrin B. WHO Classification of Tumours. Histological Type of Lung and Pleural Tumours. 3rd ed. Berlin: Springer-Verlag; 1999.
[19] Leibow AA. Bronchiolo-alveolar carcinoma. Adv Intern Med 1960;10:329-58.
[20] Okada S, Ebihara Y, Yoneyama J. Mucin-producing bronchioloalveolar carcinoma. Jpn J Lung Cancer Clin 1999;2:317-22.
[21] Goldstraw P, Crowley J, Chansky K, et al. The IASLC Lung Cancer Staging Project: proposals for the revision of the TNM stage groupings in the forthcoming (seventh) edition of the *TNM Classification of Malignant Tumours*. J Thorac Oncol 2007;2:706-14.
[22] Aokage K, Ishii G, Ohataki Y, et al. Dynamic molecular changes associated with epithelial-mesenchymal transition and subsequent mesenchymal-epithelial transition in the early phase of metastatic tumor formation. Int J Cancer 2011;128:1585-95.
[23] Karapetics CS, Khambata-Ford S, Jonker DJ, et al. *KRAS* mutations and benefit from cetuximab in advanced colorectal cancer. N Engl J Med 2008;359:1757-65.
[24] Shigematsu H, Lin L, Takahashi T, et al. Clinical and biological features associated with epidermal growth factor receptor gene mutations in lung cancers. J Natl Cancer Inst 2005;97:339-46.
[25] Bando H, Tsuchihara K, Yoshino T, et al. Biased discordance of *KRAS* mutation detection in archived colorectal cancer specimens between the ARMS-Scorpion method and direct sequencing. Jpn J Clin Oncol 2011;41:239-44.
[26] Hata A, Katakami N, Fujita S, et al. Frequency of *EGFR* and *KRAS* mutations in Japanese patients with lung adenocarcinoma with features of the mucinous subtype of bronchioloalveolar carcinoma. J Thorac Oncol 2010;5:1197-200.
[27] Kitamura H, Kameda Y, Ito T, Hayashi H. Atypical adenomatous hyperplasia of the lung: implications for the pathogenesis of peripheral lung adenocarcinoma. Am J Clin Pathol 1999;111:610-22.
[28] Kitamura H, Kameda Y, Nakamura N, et al. Proliferative potential and p53 overexpression in precursor and early stage lesions of bronchioloalveolar lung carcinoma. Am J Pathol 1995;146:876-87.
[29] Okudela K, Hayashi H, Ito T, et al. *KRAS* gene mutation enhances motility of immortalized airway cells and lung adenocarcinoma cell via Akt activation: possible contribution to non-invasive expression of lung adenocarcinoma. Am J Pathol 2004;164:91-100.
[30] Okudela K, Yazawa T, Woo T, et al. Down-regulation of DUSP6 expression in lung cancer: its mechanism and potential role in carcinogenesis. Am J Pathol 2009;175:867-81.
[31] Cloutier MM, Shaeffer DA, Hight D. Congenital cystic adenomatoid malformation. Cancer 1995;75:2844-52.
[32] Kwon YS, Koh WJ, Han J, et al. Clinical characteristics and feasibility of thoracoscopic approach for congenital cystic adenomatoid malformation in adults. Eur J Cardiothorac Surg 2007;31:797-801.
[33] Lantuejoul S, Nichlson AG, Sartori G, et al. Mucinous cells in type 1 pulmonary congenital cystic adenomatoid malformation as mucinous bronchioloalveolar carcinoma precursors. Am J Surg Pathol 2007;31:961-9.
[34] Kosaka T, Yatabe Y, Endoh H, et al. Mutations of the epidermal growth factor receptor gene in the lung cancer: biological and clinical implications. Cancer Res 2004;64:8919-23.

Bando et al. BMC Cancer 2013, 13:405
http://www.biomedcentral.com/1471-2407/13/405

BMC Cancer

TECHNICAL ADVANCE Open Access

Simultaneous identification of 36 mutations in *KRAS* codons 61and 146, *BRAF*, *NRAS*, and *PIK3CA* in a single reaction by multiplex assay kit

Hideaki Bando[1], Takayuki Yoshino[1*], Eiji Shinozaki[2], Tomohiro Nishina[3], Kentaro Yamazaki[4], Kensei Yamaguchi[5], Satoshi Yuki[6], Shinya Kajiura[7], Satoshi Fujii[8], Takeharu Yamanaka[9], Katsuya Tsuchihara[9] and Atsushi Ohtsu[1,9]

Abstract

Background: Retrospective analyses in the West suggest that mutations in *KRAS* codons 61 and 146, *BRAF*, *NRAS*, and *PIK3CA* are negative predictive factors for cetuximab treatment in colorectal cancer patients. We developed a novel multiplex kit detecting 36 mutations in *KRAS* codons 61 and 146, *BRAF*, *NRAS*, and *PIK3CA* using Luminex (xMAP) assay in a single reaction.

Methods: Tumor samples and clinical data from Asian colorectal cancer patients treated with cetuximab were collected. We investigated *KRAS*, *BRAF*, *NRAS*, and *PIK3CA* mutations using both the multiplex kit and direct sequencing methods, and evaluated the concordance between the 2 methods. Objective response, progression-free survival (PFS), and overall survival (OS) were also evaluated according to mutational status.

Results: In total, 82 of 83 samples (78 surgically resected specimens and 5 biopsy specimens) were analyzed using both methods. All multiplex assays were performed using 50 ng of template DNA. The concordance rate between the methods was 100%. Overall, 49 (59.8%) patients had all wild-type tumors, 21 (25.6%) had tumors harboring *KRAS* codon 12 or 13 mutations, and 12 (14.6%) had tumors harboring *KRAS* codon 61, *KRAS* codon 146, *BRAF*, *NRAS*, or *PIK3CA* mutations. The response rates in these patient groups were 38.8%, 4.8%, and 0%, respectively. Median PFS in these groups was 6.1 months (95% confidence interval (CI): 3.1–9.2), 2.7 months (1.2–4.2), and 1.6 months (1.5–1.7); median OS was 13.8 months (9.2–18.4), 8.2 months (5.7–10.7), and 6.3 months (1.3–11.3), respectively. Statistically significant differences in both PFS and OS were found between patients with all wild-type tumors and those with *KRAS* codon 61, *KRAS* codon 146, *BRAF*, *NRAS*, or *PIK3CA* mutations (PFS: 95% CI, 0.11–0.44; $P < 0.0001$; OS: 95% CI, 0.15–0.61; $P < 0.0001$).

Conclusions: Our newly developed multiplex kit is practical and feasible for investigation of a range of sample types. Moreover, mutations in *KRAS* codon 61, *KRAS* codon 146, *BRAF*, *NRAS*, or *PIK3CA* detected in Asian patients were not predictive of clinical benefits from cetuximab treatment, similar to the result obtained in European studies.

Keywords: Luminex assay, *KRAS*, *BRAF*, *NRAS*, *PIK3CA*, Epidermal growth factor

Background

The clinical significance of *KRAS* codon 12 and 13 mutation tests in the selection of patients with colorectal cancer who might benefit from anti-epidermal growth factor receptor (EGFR) antibodies is well established, and regulatory authorities in Europe, the United States, and Japan have recommended compulsory *KRAS* mutation testing before treatment [1-6]. Although conventional *KRAS* tests are useful to decrease treatment to nonbeneficiary populations, the efficacy of determining beneficiary populations requires improvement. The response rate to anti-EGFR antibody monotherapy among pretreated patients with tumors harboring *KRAS* codons 12 and 13 wild-type is 13%–17% [1,2], and that of combination anti-EGFR antibody and cytotoxic agent therapy is 11%–35% [5,7]. One explanation for such relatively low efficacy is that molecular alterations other than *KRAS* codon

* Correspondence: tyoshino@east.ncc.go.jp
[1]Department of Gastroenterology and Gastrointestinal Oncology, National Cancer Center Hospital East, 6-5-1 Kashiwanoha, Kashiwa, Chiba 277-8577, Japan
Full list of author information is available at the end of the article

12 and 13 mutations might confer resistance to anti-EGFR antibody therapies. Recent retrospective studies have revealed that mutations in *KRAS* codons 61 and 146, *BRAF*, *NRAS*, and *PIK3CA* are also related to resistance to anti-EGFR antibodies [8-13].

Several issues should also be considered to establish the clinical utility of expanded genome biomarker tests for anti-EGFR antibodies. First, information about the relation between mutation status and efficacy of treatment, especially among Asian populations, is still limited. Second, efficacious quality-controlled *in vitro* diagnostic kits and systems suitable for multiple genome biomarker detection are needed.

In Japan, a *KRAS* mutation assay kit based on the ARMS–scorpion method that detects seven frequently observed mutations in *KRAS* codons 12 and 13 (TheraScreen® K-RAS Mutation Kit; QIAGEN) was first approved for *in vitro* diagnostic use, and a kit using Luminex (xMAP) assay (MEBGEN KRAS Mutation Detection Kit, MBL) followed [14,15]. We recently developed another Luminex-based research-use kit, GENOSEARCH Mu-PACK, which simultaneously detects 36 mutations in *KRAS* codons 61 and 146, *BRAF*, *NRAS*, and *PIK3CA*. In addition to the hitherto approved *KRAS* codon 12 and 13 mutation kit, the multiplex kit identifies mutations by a single tube reaction using 50 ng of template DNA from formalin-fixed paraffin-embedded (FFPE) specimens.

In this study, we examined the feasibility and robustness of this multiplex kit using routine clinical samples collected from multiple hospitals. Meanwhile, we collected precise clinical data for these cases and retrospectively analyzed the relation of the mutation profiles of expanded markers to clinical outcomes following cetuximab therapy.

Methods

Patients

We screened and selected clinical and pathological data from consecutive patients who were administered either cetuximab monotherapy or cetuximab plus irinotecan between July 2008 and April 2010.

Patients who met all of the following inclusion criteria were retrospectively included in the analyses: (1) age ≥20 years; (2) histologically confirmed adenocarcinoma of the colon or rectum; (3) presence of unresectable metastatic disease; (4) baseline computed tomography (CT) performed within 28 days of initial cetuximab administration; (5) initial CT evaluation performed within 3 months of initial cetuximab administration; (6) previously documented as refractory or intolerant to fluoropyrimidines, oxaliplatin, and irinotecan; (7) Eastern Cooperative Oncology Group performance status score ≤2; and (8) adequate hematological, hepatic, and renal functions.

In the monotherapy regimen, cetuximab was administered at an initial dose of 400 mg/m^2 followed by weekly infusions of 250 mg/m^2. In the cetuximab plus irinotecan regimen, cetuximab was administered at the same dose as for monotherapy and followed by biweekly infusions of 150 mg/m^2 irinotecan, as per the manufacturer's instructions for irinotecan in Japan.

The study was conducted with the approval of the National Cancer Center Institutional Review Board, Cancer Institute Hospital of Japanese Foundation for Cancer Research Review Board, National Hospital Organization Shikoku Cancer Center Review Board, Shizuoka Cancer Center Review Board, Saitama Cancer Center Review Board, Hokkaido University Review Board, and the Ethics Committee of the University of Toyama. Written informed consent was obtained from as much patients who were alive as possible. For the deceased patients and their relatives, we also disclosed the study design at the website of National Cancer Center and gave them chances to express their wills in accordance with Epidemiological Study Guideline of Ministry of Health, Labour and Welfare in Japan.

Tissue samples and DNA extraction

Genomic DNA was obtained from primary and metastatic colorectal cancer tissues of all patients treated with cetuximab. Tissue samples harvested by biopsy or surgical resection at the participating hospitals were collected and sent to the research institution (MBL, Japan). A 2-μm hematoxylin-eosin (HE) slide and a 10-μm unstained slide were obtained from the FFPE tissue blocks; the latter was subsequently sliced into 3–10 sections. Pathological diagnoses were confirmed by a pathologist (Satoshi Fujii), with reference to the 4th edition of the WHO classification. The tumor area, determined by examining HE slides, was macroscopically dissected. Genomic DNA was isolated as described previously [16].

Luminex (xMAP) tests

A total of 36 mutations of *KRAS* codon 61 (Q61K, Q61E, Q61L, Q61P, Q61R, Q61H), *KRAS* codon 146 (A146T, A146S, A146P, A146E, A146V, A146G), *BRAF* codon 600 (V600E), *NRAS* codon 12 (G12S, G12C, G12R, G12D, G12V, G12A), codon 13 (G13S, G13C, G13R, G13D, G13V, G13A), codon 61 (Q61K, Q61E, Q61L, Q61P, Q61R, Q61H), *PIK3CA* exon 9 codon 542 (E542K), codon 545 (E545K), codon 546 (E546K), and exon 20 codon 1047 (H1047R, H1047L) were analyzed using Luminex (xMAP) technology (GENOSEARCH Mu-PACK, MBL, Japan).

First, 50 ng of template DNA collected from FFPE tissue samples was amplified by polymerase chain reaction (PCR) using a biotin-labeled primer. Thereafter, the PCR products and fluorescent Luminex beads (oligonucleotide probes complementary to wild and mutant genes were bound to the beads) were hybridized and labeled with streptavidin–phycoerythrin. Subsequently, the products

were processed by Luminex assay and the collected data analyzed using UniMAG software (MBL, Japan). The procedure time was approximately 4.5 h.

We also used the Luminex assay kit (MEBGEN KRAS Mutation Detection Kit, MBL, Japan) currently approved for clinical use by the Ministry of Health, Labour and Welfare of Japan [16] to detect *KRAS* codon 12 and 13 mutations.

Direct sequencing methods

In addition, to confirm the mutations detected by the Luminex assays, the same mutations of *KRAS* codons 61 and 146, *BRAF*, *NRAS*, and *PIK3CA* were analyzed by direct sequencing. A total of 700 ng of template DNA was used for these PCR reactions and the PCR products were directly sequenced with the same primers used for PCR. A BigDye Terminator v3.1 Cycle Sequencing Kit and an ABI PRISM 3730xl DNA Analyzer (Life Technologies) were used. Analyses of DNA sequences were performed using Sequencher (GeneCodes).

Statistical analysis

Response rates (RRs) and disease control rates (DCRs) (including complete or partial response and stable disease) were evaluated as per the Response Evaluation Criteria in Solid Tumors (RECIST) (version 1.0). Progression-free survival (PFS) was defined as the time from initial administration of a cetuximab-containing regimen to either the first objective evidence of disease progression or death from any cause. Overall survival (OS) was defined as the time from initial administration of a cetuximab-containing regimen to death from any cause. RRs, DCRs, PFS, and OS of all patients were re-evaluated by the principal investigators at each institution. The relative dose intensity was defined as the ratio of the actual dose administered to the planned dose.

Fisher's exact test and the Kruskal–Wallis test were used to compare patient characteristics, relative dose intensity, and treatment response. PFS and OS data were plotted as Kaplan–Meier curves, and differences among the groups according to *KRAS*, *BRAF*, *NRAS*, and *PIK3CA* gene status were compared using the log-rank test and hazard ratio calculated from a Cox regression model with a single covariate. All analyses were performed by a biostatistician (Takeharu Yamanaka), using IBM SPSS® Statistics 21 package software (SPSS Inc., Tokyo, Japan).

Results

Concordance between Luminex and direct sequencing

From September 2008 to April 2010, 376 patients were treated with a cetuximab-containing regimen at seven institutions. Of these, 83 patients met the inclusion criteria and specimens were collected from them for analysis (232 patients did not meet the inclusion criteria and 61 specimens could not be collected). We collected 78 surgically resected specimens and 5 biopsy specimens, from which the median amount of template DNA collected was 25,114 ng (range: 2740–84,738) and 1691 ng (range:1469–2668), respectively (Table 1).

One patient's gene status could not be detected by either Luminex or direct sequencing because DNA harvested from the resected metastatic liver specimens could not be amplified by PCR. In the remaining 82 patients, the concordance rate for mutations between the 2 methods was 100% (Table 2).

Among the 82 specimens, 3 *KRAS* codon 61 mutations (3.6%), 2 *KRAS* codon 146 mutations (2.4%), 4 *BRAF* mutations (4.9%), 2 *NRAS* mutations (2.4%), and 4 *PIK3CA* mutations (4.9%) (1 in exon 9 and 3 in exon 20) were detected using both the expanded kit and direct sequencing. Moreover, we identified 15 *KRAS* codon 12 mutations (18.3%) and 6 *KRAS* codon 13 mutations (7.3%); in total, 21 samples (25.6%) with *KRAS* codon 12 or 13 mutations were detected by using the *KRAS* Luminex assay kit. All mutations except for *PIK3CA* were mutually exclusive (Table 2, Figure 1).

Patient characteristics

Clinical data were collected from 83 patients. We used data from 82 patients whose genomic DNA could be successfully examined using both the expanded kit and direct sequencing. Six of the 82 patients were treated with cetuximab monotherapy, while the remaining 76 were treated with a regimen of cetuximab plus irinotecan.

Of these 82 patients, 49 had tumors with no mutation (all wild type), 21 had tumors with mutation of either *KRAS* codon 12 or 13, and 12 had tumors with mutation of either *KRAS* codon 61, *KRAS* codon 146, *BRAF*, *NRAS*, or *PIK3CA*. No significant difference was observed in the characteristics of these three groups except for the ratio of refractoriness to intolerance of prior oxaliplatin (Table 3).

Table 1 Template DNA harvested from FFPE specimens

	Surgically resected	Biopsy	Total
Number of specimens	78	5	83
Total amount of template DNA (ng) [median (range)]	25,114 (2,740–84,738)	1,691 (1,469–2,668)	22,591 (1,469–84,738)
Amount of template DNA per slice (ng) [median (range)]	8,371 (914–28,246)	370 (154–889)	7,530 (154–28,246)